A STUDY OF THE INFLUENCE OF LARGE WIRE DRAWING PLASTIC STRAINS ON DISLOCATION SUBSTRUCTURES AND MECHANICAL PROPERTIES OF ALUMINUM AND ITS DILUTE ALLOYS

A THESIS

Presented to

The Faculty of the Division of Graduate Studies

by

Shailendra K. Varma

In Partial Fulfillment

of the Requirements for the Degree

Doctor of Philosophy in the School of Chemical Engineering

Georgia Institute of Technology

August, 1977

A STUDY OF THE INFLUENCE OF LARGE WIRE DRAWING PLASTIC STRAINS ON DISLOCATION SUBSTRUCTURES AND MECHANICAL PROPERTIES OF ALUMINUM AND ITS DILUTE ALLOYS

Approved:

Bruce G. LeFevre, Chairman

Edgar A. Starke Jr.

David Kalish

Date Approved by Chairman 11-16-77

ACKNOWLEDGEMENTS

The author wishes to express his sincerest appreciation to his advisor, Dr. B. G. LeFevre, for his many significant contributions to the work performed for this thesis. The technical discussions with the thesis reading committee members, Dr. E. A. Starke, Jr. and Dr. David Kalish, are greatly appreciated.

I am very grateful to Mr. Ron Adams of Southwire Company, Carrollton, Georgia for his help in the processing of materials used in this research. The technical assistance of Mr. J. W. Elling of Bell Telephone Laboratories in the mechanical testing. was essential to this work.

TABLE OF CONTENTS

LIST OF TABLES

LIST OF ILLUSTRATIONS

FIGURE Page

FIGURE Page

SUMMARY

The relationship between microstructure and strain hardening was studied for aluminum and its dilute alloys subjected to room temperature wire drawing deformations to the strains of 5. The materials studied were pure aluminum, Al-0.2Mg, Al-0.6Fe and EC aluminum. The additions of Mg and Fe were made to determine separately the effects of small amounts of soluble and insoluble alloying elements. Complete stress-strain curves were obtained at various wire drawing intervals and structures were characterized by transmission electron microscopy, selected area diffraction and x-ray diffraction.

In all the alloys studied changes in either strength level or microstructure continued to take place to wire drawing strains of 5. After initial rapid strengthening, pure aluminum, Al-0.2Mg and EC aluminum shows continued linear hardening while Al-0.6Fe shows work softening at $\varepsilon = 2.3$. The accompanying microstructures evolved, in all cases in the following sequence: formation of a dislocation cell structure, cell size refinement, subgrain formation and dynamic low temperature recrystallization (DLTR). The cell and subgrain structures are characterized by low angle boundaries and the DLTR structure by high angle boundaries. Although detailed microstructure studies were not made beyond $\varepsilon = 5$, additional strain hardening data indicates saturation and possible steady state conditions at strains of approximately 7 for pure aluminum. This behavior differs from that

of high temperature deformation of dilute aluminum alloys where a steady state low angle subgrain structure (and constant flow stress) is achieved at moderate strains and dynamic recrystallization does not occur.

In the materials studied, dislocation cell structure occurs in the size range of 1 to 0.45μ and subgrains from 0.45 to 0.25μ. Two distinct modified Hall-Petch relations are required for these two regions. The subgrains are less effective as strengthening barriers, hence a single flow stress vs substructure size relationship should not be rigorously applied. The strengthening effect of subgrains produced during cold drawing is roughly equivalent to those produced by static annealing. The small additions of soluble and insoluble impurities affect the rate of substructure formation and refinement but not the relationship between substructure and strength.

When the complete stress-strain curves at various wire drawing intervals are fit to the Hollomon equation $\sigma = K\varepsilon^n$, K and n have been shown to be structure sensitive and insensitive respectively. K is found to vary inversly with the average cell size.

CHAPTER I

INTRODUCTION

The influence of dislocation substructure on mechanical properties of alloys has long been recognized and is receiving renewed attention [1-5]. Substructures formed by various mechanical thermal processes have been shown to affect ambient and elevated temperature flow stress [2, 4, 7-17], instantaneous creep rate [8, 18-21] and high cycle fatigue life [22]. Extensive studies have been carried out in the hot deformation and creep regimes on the interrelation between substructure, steady state flow stress, strain rate, temperature and alloying additions. In addition the evolution of dislocation substructures with small to moderate strains at room temperature is well documented. An area which has received relatively little attention is that of large strains ($\varepsilon > 1$) at low temperatures ($T < 0.3T_m$) where dynamic recovery is limited essentially to cross slip.

Recent work on the hardening and evolution of substructures during large strain deformation at low temperature [9, 14, 15, 23-29] has highlighted areas that warrant further investigation. These include:

a. The extent of continued hardening and associated changes in dislocation cell size, shape and orientation.

b. Differences in work hardening modulus and substructure refinement between BCC, FCC and HCP metals.

c. The influence of the type of deformation process on work hardening characteristics.

d. The influence of the initial microstructure on the subsequent hardening characteristics and substructure.

e. Stages of extensive dynamic recovery and formation of high-angle boundary structures at very large strains at room temperature [12, 13, 27, 28].

f. The influence of alloying additions (soluble and insoluble) and deformation process on Hall-Petch constant for dislocation cell boundary strengthening.

Most of the detailed microstructural studies of low temperature, high strain deformation have been conducted on BCC Fe alloys. This study deals with certain high stacking fault energy FCC metals: aluminum and its dilute conductor grade alloys. The objective is to provide a better understanding of the dislocation substructures and its relationship to work hardening behavior during heavy cold drawing. The samples were chosen so as to separately evaluate the effects of small additions of soluble and insoluble alloying elements, Mg and Fe respectively. The work has practical significance in the application of conductor grade aluminum alloys in power and signal transmission lines. Strength, which is an important requirement, can be obtained only to a very limited extent by alloying because of the conductivity requirements. Improvements in mechanical properties are therefore largely dependent on processing variables, the most prominent of which is the drawing operation.

CHAPTER II

LITERATURE SURVEY

Dislocation Substructures: General

Mechanical-thermal processing and the formation of dislocation substructures as a means of controlling mechanical properties has recently been reviewed in detail [1-7]. The combined effects of deformation and recovery (dynamic or static) tends to produce a dislocation cell or subgrain structure (a strict distinction between cells and subgrains is not made in the literature, but the term 'subgrain' is generally applied to more well-defined and coarser structures produced at elevated temperature) which is characteristic of the alloy and process conditions. Ideally the parameters which would define the substructure are: (a) cell size, (b) cell shape, (c) overall dislocation density, (d) cell misorientation, (e) cell wall character and (f) cell interior dislocation density. The factors which determine these features are: (a) total plastic strain, (b) strain rate, (c) deformation temperature, (d) crystal structure, (e) composition and (f) pre-post or intermediate annealing conditions. Other related factors such as flow stress, stacking fault energy, operating slip systems, texture, etc. are dependent on these. The softening mechanisms and the extent to which they operate are very much dependent on temperature. The microstructures produced under

steady state conditions at elevated temperatures (i.e. warm or hot working and creep) differ in some important details from those produced in cold forming. Although this work is concerned with the latter, it is both instructive and convenient to first consider structures produced at elevated temperatures.

High Temperature Deformation

Deformation mechanisms and related microstructures under hot forming and creep conditions have been extensively reviewed by McQueen and Jonas [5]. The softening processes accompanying or succeeding plastic flow are: static recovery, dynamic recovery and static dynamic or metadynamic recrystallization. In the case of high stacking fault energy metals under conditions where dynamic recovery can effectively suppress the dynamic recrystallization (e.g., low strain rates) a steady state dynamic equilibrium can exist between the multiplication and annhilation of dislocations. A steady state flow stress and microstructure consisting of equiaxed subgrains is then maintained independently of the total strain. All microstructural features remain constant from this point including total dislocation density, subgrain size, shape, wall character and misorientation. The structure accommodates further strain either by boundary migration [30] or by coalescence and reformation [5]. For a given composition the steady state flow stress is a function of temperature and strain rate. Consequently the associated characteristic substructure may be related with either the temperature corrected strain rate [2] or

the modulus compensated flow stress [2, 4, 13]. Higher temperatures and lower strain rates result in larger subgrains [13, 16, 31]. The higher temperature subgrains also have fewer internal dislocations and sharper boundaries of fewer redundant dislocations. A modified Hall-Petch relation has been applied to relate the room temperature yield strengths with subgrain sizes developed at elevated temperatures during the deformation.

$$\sigma = \sigma_o + k\, d^{-m} \qquad (1)$$

where σ and d are the yield strengths and subgrain sizes respectively while σ_o, k and m are constants. It has been found that m generally varies between $\frac{1}{2}$ and 1 while in most of the cases the data fits best with a value of 1 [8, 13-15]. The value of k is affected by deformation temperature [4] and alloying [1,5]. Young and Sherby [4] have found that in FCC and BCC Fe a single constant relates the cell size to flow stress independent of crystal structure and solid solution alloying. For the case of aluminum alloys [2], however, k has been shown to be a function of Mg content. The affect of alloying on k therefore appears to depend on the system. The values of k for grain boundaries are normally higher than those of subgrains on a plot with $m = \frac{1}{2}$. For similar cell and grain sizes below one micron, however, strengthening achieved by subgrains is substantially higher [4, 5, 8].

Quantitative models have been developed relating dislocation density to subgrain size by Kuhlman-Wilsdorf [32] and Holt [33]. Under the conditions for which flow stress is related to the statistical dislocation population [13, 34, 35], the m = 1 flow stress can be

rationalized. The value of k for room temperature yielding may be related to the subgrain boundary character and associated source lengths [6, 35-37]. Ideally σ_o should represent the tensile flow stress of a single crystal free of substructures and oriented for polyslip [20]. Values obtained by extrapolation may be negative. This indicates that although the modified Hall-Petch relation may be derived from various strengthening models it is still somewhat empirical.

Low Temperature Deformation

As the deformation temperature is lowered recovery mechanisms become less active with the result that cell structures are increasingly less dependent on temperature and more dependent on the type and extent of deformation. Below $0.5T_m$, the cells tend to be elongated, less well defined, smaller and their size mush less sensitive to the deformation temperature [13, 16, 38]. Below $0.3T_m$ recovery is virtually limited to cross slip so that steady state is not achieved except under certain conditions at very large deformation [23, 39-49] or cyclic straining [50]. Because of this, the extent of cellular formation and refinement is very much a function of the stacking fault energy.

Important differences exist between the substructures produced at high and low temperatures. For example, the steady state microstructures at elevated temperatures result in a final fixed cell size regardless of total strain whereas continued cellular refinement may occur to strains of 7 or better at room temperature depending on the material

[12, 23, 25, 27, 29]. In addition, the cellular misorientations at elevated temperatures stablize at less than 10 degress [1, 51-53] whereas large misorientations [15] and high angle boundaries [12, 27] may eventually evolve with large strains at low temperatures. In addition, the shape of the low temperature cells is dictated by the interrelation between operating slip systems, texture and external shape change [15, 25, 47, 48]. Finally, steady state substructures developed at elevated temperatures are characteristic of temperature, strain rate and composition only while low temperature substructures may depend on the starting microstructure even to relatively large strains 29 . These differences are compounded by the fact that the combination of deformation and recovery at elevated temperatures result in microstructures which can not be duplicated by low temperature deformation followed by annealing.

The evolution of dislocation substructures at low to moderate strains at room temperature (e.g., by tensile deformation to fracture) is well documented and has been reviewed by McElroy and Szkopiak [1]. One of the primary variables is stacking fault energy (SFE). High SFE metals initially form dislocation tangles ultimately link up into boundaries outlining reasonably well-defined cells. The cell structure becomes noticeable at some intermediate amount of strain depending on the mode of deformation and the particular alloy characteristics. The cell walls consist of rather diffuse ill-defined Frank networks. With further deformation this structure is refined and sharpened while the metal continues to harden. In the case of tensile deformation a stable cell size is reached from which point

work hardening proceeds at a lower rate as the dislocation density continues to increase. During the later stage of hardening, cell walls become sharper, the cell interiors become more dislocation free and the average misorientation between cells increases although it remains low (a few degrees at most). True steady state is not achieved, however, and the total strain to fracture is quite low in comparison to that which can be achieved by deformation techniques such as rolling, swaging, torsion, compression and drawing.

The microstructure and properties achieved by these and other large strain methods appear to differ. Published work in this area is rather limited, but is available on: wire drawing in BCC iron alloys [13, 15, 24-26, 41], austenitic steel [26], Cu [26] and Ti [54], torsional deformation in BCC Fe-Ti [23] and Cu [42], compression in Fe [42], Cu [44] and U [43], rolling in FCC Cu base alloys [9, 27, 28, 55] and Al [27], rolling and wire drawing in BCC Nb [45] and wire drawing in Al alloys [12, 29, 46, 57, 58].

It is generally assumed that the behavior of FCC metals is fundamentally different from BCC metals at large strains because of the extent of dynamic recovery during deformation. Several authors [26, 42, 44, 49] have indicated that a steady state microstructure and hardness are reached at large strains. The work of Nutting et al. [9] further suggests that substructural development takes place in fairly distinct stages as follows: the formation of cells; strain induced recovery with increasing misorientation to 5-10°; formation of nearly dislocation free, equiaxed small grains with high-angle boundaries; strain induced grain growth. The last two stages are

equivalent of strain induced recrystallization (beginning at around strain of 5) and are accompanied by softening and changes in work hardening parameters.

These results taken collectively may be summarized as follows:

a. Texture development, subgrain formation and macroscopic shape changes are interrelated. Consequently different substructural details and hardening behaviors can be achieved at same equivalent strains by varying either the deformation mode or the alloy.

b. It is possible to obtain continued hardening without saturation (e.g., by wire drawing BCC Fe) to the highest strains of 10. Hardening is accompanied by continued refinement of cell size and increasing misorientation to very large angles.

c. Achievement of steady state conditions after large low temperature strains have been shown and may be a general affect in FCC metals (including wire drawing). FCC metals also show evidence of work softening at high strains which may be associated with low temperature dynamic recrystallization [9, 27, 28].

d. The tensile strength of heavily deformed specimens can be related to a modified Hall-Petch equation similar to that for subgrains. Fixed values of σ_o, k and m can be made to fit structures produced over a wide range of strains in a given materials (e.g., strains from 0 to 7 in Fe). A value of -1 for m can be applied to a variety of structures including those containing cells of high misorientations [12, 14, 15, 24, 25, 29].

e. The character of cell walls, and therefore the values of σ_o and k may change with the mode of deformation, composition or

post annealing. Within a given alloy they may also be affected by the initial microstructure at least to the strains of nearly 3 [29].

Influence of Texture

The influence of texture and mode of deformation on the substructure at high strains has not been analyzed in detail although certain points have been clarified. The following factors must be considered as well as their interdependence: (a) The macroscopic shape change during deformation, (b) uniformity of deformation and associated redundant strain [59], (c) the rate of dynamic recovery, (d) effect of texture in conjunction with (a) - (c) on the formation of the substructure and (e) effect of tecture as an orientation factor on the strength during deformation. The example of wire drawing in BCC Fe is reasonably clear [15, 25].

A strong <110> fiber texture results in slip being favored in two directions so that plastic flow can occur locally by plain strain conditions. The axisymmetric microscopic flow is accommodated by the formation of elongated cells which are continually refined through the process of polygonization and tend toward pure tilt boundaries of 90° misorientation [14]. This is accompanied by continued linear hardening to the strains of 7. On the other hand when the mode of deformation is changed from wire drawing to torsion or compression, BCC iron tends to approach a steady state strength and structure [43, 47, 48, 54]. Young, Anderson and Sherby have compared the tensile flow stress for a given cell size under torsion and wire drawing. It results in the same flow stress under tension.

Thus it is speculated that texture influences the substructure but does not contribute directly to the strength in the case of BCC iron. This has been explained on the basis of redundant strain associated with the different modes of deformation. Attempts are being made to explain the phenomenon on the basis of total equivalent strains, but none of these methods result in an ideally homogeneous deformation.

Relationship of Substructure to Tensile Flow Stress

This subject has been discussed by various investigators in some detail; however, much of the experimental and theoretical work relates to cell or subgrain boundaries produced either by high temperature steady state conditions or low temperature light deformation. For structures produced by large strains at low temperature it has been shown that initial yielding can be correlated with a modified Hall-Petch equation for which m = 1 (eq. 1) [12, 14, 15, 23-25, 29, 57]. Various interpretations may be placed on k and m regarding cell boundary character.

The correlation of flow stress with an expression of the form of equation 1 is an oversimplification of the work hardening characteristics of polycrystalline materials [34, 60]. It may be derived from an association of the mean slip length (λ_s) with cell size, however a functional relationship between λ_s, d and ε would be needed for a description of the complete stress-strain curve. Thompson and coworkers [34] have shown that λ_s asymptotically approches the measured cell diameter during tensile testing of high stacking fault FCC metals. This is an indication that cell boundaries tend

toward impenetrable barriers with increasing strain. Langford and Cohen [15] have developed analysis for tensile yielding in cell structures developed through large strains. In their analysis the microstructure consists of a mixture of penetrable and impenetrable cell boundaries differentiated by some critical misorientation angle. Their strength contributions were evaluated and added in such a way as to be consistent with the modified Petch relation.

Another approach to tensile yielding in well-defined subgrain (or cell) structures is to relate shear flow stress τ_f to the dislocation source length of the boundary [6, 32, 37, 61]:

$$\tau_f = K' \frac{Gb}{\ell_s} \tag{2}$$

where b is the Burger's vector, K' the proportionality constant, G is shear modulus and ℓ_s the dislocation source length. Such an analysis obviously requires detailed knowledge of boundary character and to date has been used only semi-quantitatively.

There has been extensive work done in the use of Hollomon equation for fitting the tensile stress-strain curves of different grain sizes [62]. The Hollomon equation in its simplest form is described as follows:

$$\sigma = K \varepsilon_p^n \tag{3}$$

where σ is the true stress, ε_p is the true plastic strain while K and n are constants. Morrison in his treatment with several different steels related the strengthening exponent 'n' and coefficient 'K' to

grain size and obtained a relation between these parameters. In certain cases he observed that the stress-strain curves could be best fitted with two values of n instead of one. The two values of n were explained in terms of the differences in microstructure where first n corresponds to equiaxed subgrains while second n is characterized by the formation of elongated subgrains in the direction of the tensile axis. K was found to be structure sensitive. An inverse proportionality was established between K and grain size. Cairns et al. [9] observed that K and n were structure sensitive in pure Cu where a systematic variation in K and n related to the changes in substructure during drawing. The Hollomon constants have not been related to cell sizes so far in the literature. This will be an area that will be explored in the present investigation. There have been many modifications to the Hollomon equation made to date [63 - 68].

Effects of Alloying Additions

The effect of alloying elements in solid solution increases the yield strength, refines the microstructure, offers resistance to the rotation and motion of subgrains [58] and lowers the SFE of the metal which reduces cross slip. However, in some alloys the solute atom has either no affect or even increases the neatness and cell size [17] e.g., in Al-Mg [69], Ni-Fe [70], Ni-base superalloys [71] and some iron alloys having Si, Cr and Ni [72]. In the case of Al-Mg system, Mg also increases the resistance to annealing by the formation of solute atmospheres [73]. The addition of solutes in solid solution lowers the stacking fault energy of the metal which

delays the formation of dislocation tangles and cells to relatively higher strains during the deformation process. Al-0.2Mg alloy will be studied in this investigation to follow the changes in substructure due to the presence of solutes in solid solution during wire drawing deformation at room temperature.

In the presence of dispersed, incoherent second phase particles in alloys, the cell size is a function of dispersion spacing [17]. These particles can reduce the process of coalescence of cell boundaries during annealing due to pinning of the cell walls [57]. The effect of these particles is to reduce the cell size and increase the dislocation density during the deformation. Uniform distribution of the particles has been shown to be an important factor for the production of small and stable subgrain structure in an Al-Fe-Co system [58] during wire drawing. Iron has essentially no solubility in aluminum, although as much as 0.17% can be retained in solution during rapid solidification, and forms stable intermetallic compound $FeAl_3$ ($FeAl_6$ is an unstable compound formed during rapid solidification of the alloy from the melt). Deformation during wire drawing of an Al-0.60Fe alloy will be studied in this investigation in order to follow the changes in substructure due to the presence of second phase particles.

Summary: Large Strain, Low Temperature Substructure Strengthening

From the previous discussion it is clear that certain questions regarding large strain, low temperature deformation remain to be answered. The primary questions are:

i) Are there fundamental differences between BCC, FCC, and HCP metals in the large strain region? (e.g., is the achievement of a steady-state structure or the onset of dynamic recrystallization at large strains truly characteristic of FCC metals or simply a function of the deformation mode?)

ii) To what extent are the structure and hardness at large strains affected by the mode of deformation and the stacking fault energy?

iii) To what extent do cellular refinement shape change and misorientation continue with deformation? Are steady-state microstructures or the equivalent of dynamic recrystallization achieved at large strains?

iv) How do parameters from modified Hall-Petch and Hollomon relations (obtained from interval tensile tests) correlate with microstructure and strain? Do they change discontinuously with strain and thereby indicate distinct stages of microstructural development? Are different values required for structures produced by different types of deformation?

v) What is the contribution of texture strengthening as an orientation factor, to the tensile flow stress and how much is attributable to the substructure per se?

vi) How are the above affected by soluble and insoluble alloying additions?

CHAPTER III

EXPERIMENTAL PROCEDURES

Dilute alloys of aluminum, Al-0.2Mg and Al-0.6Fe, were prepared from high purity aluminum in the form of a rod of 3/8 inch diameter. The rods were cold drawn on a set of dies to obtain a final reduction corresponding to a true strain of 4.95 and wire diameter of 0.032 inch. Several intermediate reductions were taken during wire drawing and tested under tension for mechanical properties. Complete tensile stress-strain curves were obtained for each reduction in wire drawing. The substructural details were examined using optical microscopy and TEM. Wire texture was determined by the use of x-ray transmission pinhole patterns. Details of these experimental procedures will be described in this section.

Alloy Preparation

The starting material for each alloy except commercial grade electrical conductor aluminum was 99.999% pure aluminum. The alloying additions were made in the form of master alloy. The high purity aluminum was melted in an induction furnace using 95% pure alumina crucible. After the complete melting was ensured, the alloying additions were made and stirred well to enhance complete homogenisation of the alloy. The melt was poured at a temperature of 1350°F into a metal mould. The result of the casting was a bar of 1½ inches in

diameter and 16 inches in length. This cast bar was hot rolled resulting in a product of 3/8 inch diameter rod. These rods were annealed for 3 hours in a furnace at 800°F and the samples were air cooled. The spectroscopic analysis in Table 1 indicates the final compositions of the four materials used in this study. The compositions are given weight percents.

The air cooled rods of 3/8 inch diameter were drawn on a one die drawing machine at 42 feet per minute. Heating of the wires during wire drawing was minimized by the continuous flow of the lubricant oil at the inlet tip of the die. The dies were made of silicon carbide with an approach angle of 16 degrees.

Mechanical Testing

Tensile tests were conducted on an Instron machine (model no. 1251) at a crosshead speed of 2 mm/minute. A strain gage extensometer with one inch gage length and capable of recording 50% elongation was used for the determination of stress-strain curves. A minimum of three stress-strain curves with failure inside the extensometer were obtained for each sample.

Optical and Transmission Electron Microscopy

The samples to be examined under optical microscope were mounted in quick mount in order to minimize the heating involved in the conventional bakelite mounting. After mechanically polishing on a series of coarse grit papers, the final mechanical polishing was performed on a vibromat using 0.05 micron alumina powder in

water in the form of paste. To minimize the fine scratches on the surface of the specimen, and electropolishing treatment was given to the samples using a solution of nitric acid and methanol in the ratio of 1:3 at 20 volts for five seconds. All the optical microscopy was performed on an anodized surface. The anodizing was done in a solution of 4.5% by volume of hydrofluroboric acid in water using lead cathode at 20 volts. The optical microscopy was performed on a Vickers metallograph equipped with polarized light.

The foils from the cross section of the wires were made by cutting small discs of nearly 0.020 inch thick with Buehler Isomet Low Speed saw. The discs were mechanically thinned to a thickness of 0.012 inch. These wafers were dimpled on both sides using a jet polishing apparatus. The solution used for dimpling was a mixture of nitric acid and methanol in the ratio of 1:3 at 300 volts. The resulting thickness from the dimpling was about 0.002 inch in the center of the wafers. The final electropolishing was performed in the same solution at 14 volts. The electrolyte was cooled to less than -20°C. Stainless stell was used as a cathode. The electropolishing was stopped as soon as a small hole appeared in the center of the foil, after which the foil was carefully washed in chilled methanol. The substructures of the foils were analysed by the standard TEM methods of bright field imaging and selected area diffraction (SAD) patterns. The electron microscopy was performed using both Siemens Elmiskop 1A and JEOL microscopes equipped with a double stage tilting device.

Wire Texture Determination

The texture of the wire was determined by taking several x-ray transmission pinhole patterns. The pinhole patterns were taken on both as drawn and polished surfaces of the wire. The wire axis was kept perpendicular to the x-ray beam. Mo radiation at 50kv and 40mA was used to get the pinhole patterns.

TABLE 1

Spectrograph Analysis (in % weight)

	Fe	Ni	Zn	Mn	Cr	Ga
Pure Aluminum	<0.005	<0.001	<0.002	<0.001	<0.001	<0.001
Al-0.2Mg	<0.005	<0.001	<0.003	<0.001	<0.001	<0.001
Al-0.6Fe	0.640	<0.001	<0.003	<0.001	<0.001	<0.001
EC Aluminum	0.075	0.003	0.009	0.002	0.002	0.001

	Si	Ti	V	Mg	Cu
Pure Aluminum	<0.003	<0.001	<0.003	<0.001	<0.001
Al-0.2Mg	<0.003	<0.001	<0.002	0.002	<0.001
Al-0.6Fe	<0.003	<0.001	<0.002	<0.001	<0.001
EC Aluminum	0.050	0.001	0.002	0.001	0.001

CHAPTER IV

RESULTS AND DISCUSSION

The strain hardening and substructural changes during wire drawing of high purity aluminum, Al-0.2Mg, Al-0.6Fe and EC aluminum is discussed in this section. Hardening up to true strains of 4.95 will be related to microstructural details such as subgrain sizes, boundary character, misorientation angles and textures. Finally a model describing various stages of substructures and the relationships to tensile flow stress will be presented.

Pure Aluminum

The starting material for the high purity aluminum study was a rod of 3/8 inch diameter which had been hot rolled and fully annealed. Figure 1 is an optical micrograph of a longitudinal section of this rod showing it to be fully recrystallized. Figure 2 is an electron micrograph showing the dislocation configuration around a grain boundary. It indicates a complete absence of cells for the starting condition.

The rod was cold drawn (see experimental procedures for details) to obtain a final reduction corresponding to a strain of 4.50 and wire diameter of 0.040 inch. Figure 3 illustrates the strain hardening envelope obtained from tensile tests conducted

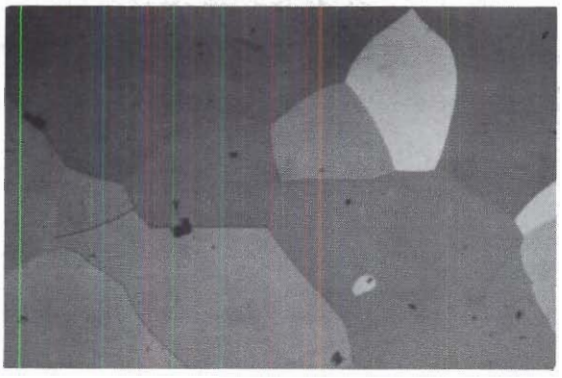

Figure 1. Optical Micrograph of Pure Aluminum Rod, Annealed for 3 Hours at 800°F, on its Longitudinal Section X40

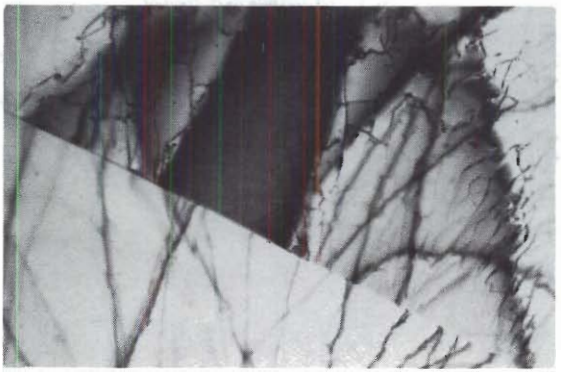

Figure 2. TEM of Pure Aluminum Rod, Annealed for 3 Hours at 800°F, on its Transverse Section

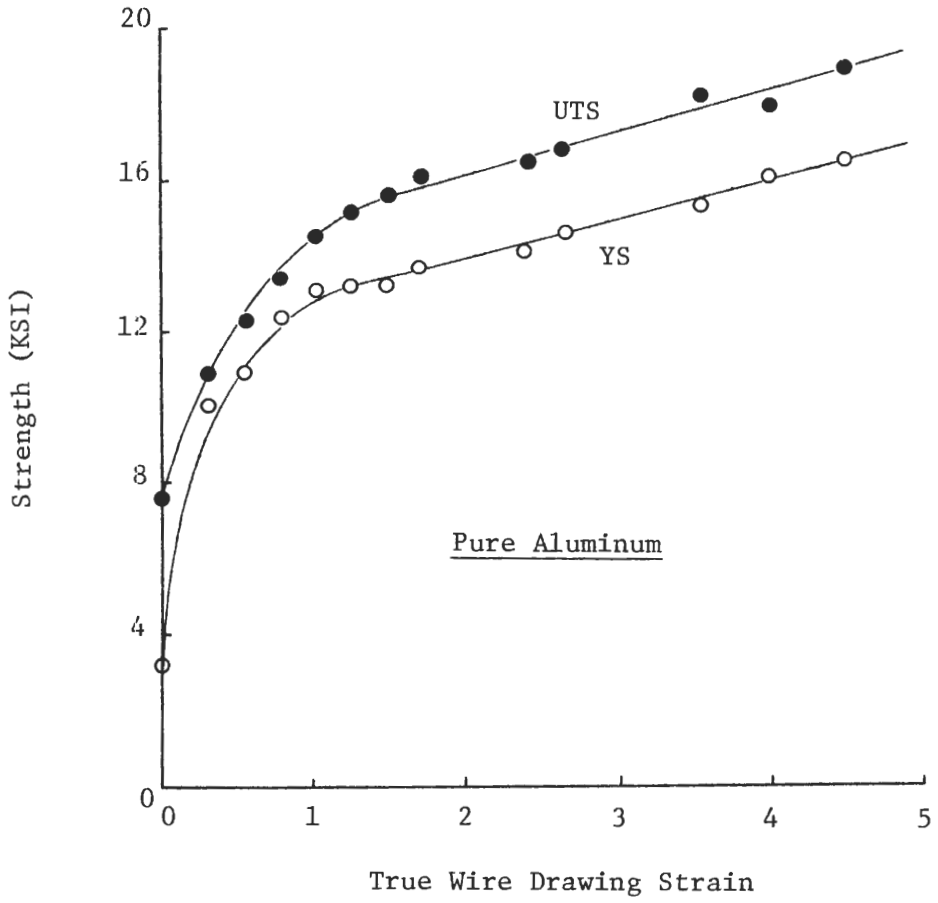

Figure 3. Strain Hardening Envelop of Cold Drawn Pure Aluminum

at various drawing intervals. The 0.2% yield strength increases very rapidly in the initial stages up to a strain of 0.5. Between strains of 0.5 to 1.5 the hardening rate continues to decrease and finally a constant hardening rate up to a total strain of 4.5 is observed. The strain hardening modulus for pure aluminum (1.0 KSI) in the high strain region is found to be extremely low when compared with Fe [25] and Cu [9] where values of 20.5 and 7.5 KSI respectively have been reported. Unusual hardness fluctuations in aluminum after a reduction of 75% thickness have been reported by Howard [56]. Another study on cold rolling of aluminum [27] indicates a decrease in tensile strenth after a strain of 3. Differences between these results and the present study may be due to either the purity of aluminum or adiabatic heating during the deformation.

Microstructural characterization during wire drawing was carried out by both optical microscopy and TEM. Fine microstructural changes could not be resolved optically after a strain of 1 and were carried out exclusively by TEM in this region. For very low strains, the optical micrographs showed elongation of grains in direction of wire drawing and inhomogeneous microstructures which are characteristics of the deformation process. A distinct cell structure was observable by TEM only after a strain of 0.5. The cell size variations over the entire strain range up to 4.5 is shown in Figure 4. The bars indicate the maximum and minimum observed values of cell sizes. Between strains of 0.5 to 1.5 the

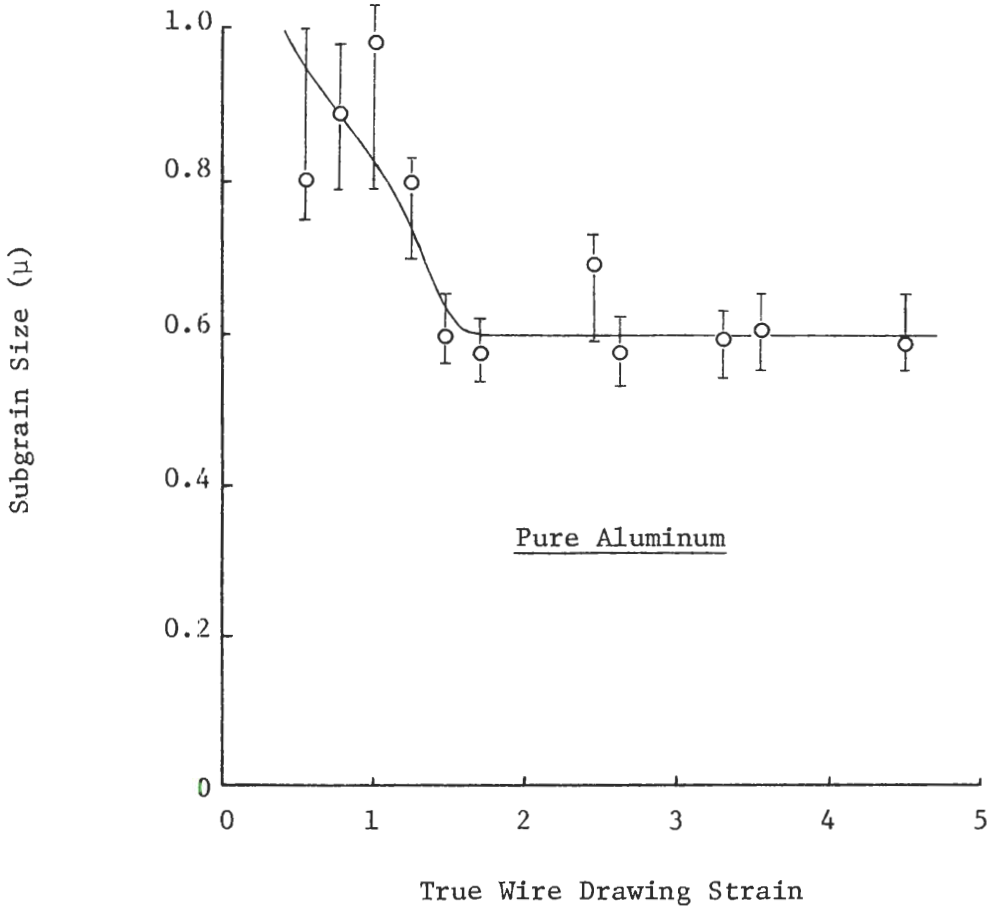

Figure 4. Variation of Cell Size as a Function of True Wire Drawing Strain in Pure Aluminum

cell size decreases with increasing strain. Figure 5 shows the cell structure characteristic of these strains. Along with the decreasing size there is a sharpening of the boundaries. After a strain of 1.5 the average size almost remains essentially constant up to the strain of 4.5. Although the average cell size remains constant during this stage the boundary character does not. Some of the boundaries show a distinct sharpening to appear as high angle boundaries while other apparently newly formed boundaries are similar in appearance to those at $\varepsilon = 0.5$. The dual character is indicative of the competition between deformation, dynamic recovery and dynamic low temperature (DLT) recrystallization during a stage of linear hardening and constant average cell size. All the alloys in this study exhibited DLT recrystallization and the formation of high angle boundaries at high strains. The term "cell" will continue to be used for simplification although the boundaries in the high strain region are a mixture of cell, subgrain and grain. These stages will be discussed more fully in following sections.

From a comparison of the strain hardening and cell size curves it appears that structure-property changes during room temperature drawing of high purity aluminum occurs in stages. It is clear that no general Petch-type relationship can be established over the full range of strains investigated due to changes in one or more of the following: (i) cell boundary character, (ii) cell misorientation, or (iii) texture. Factors

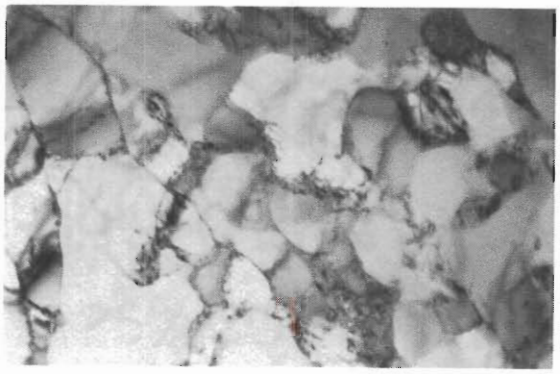

(a)

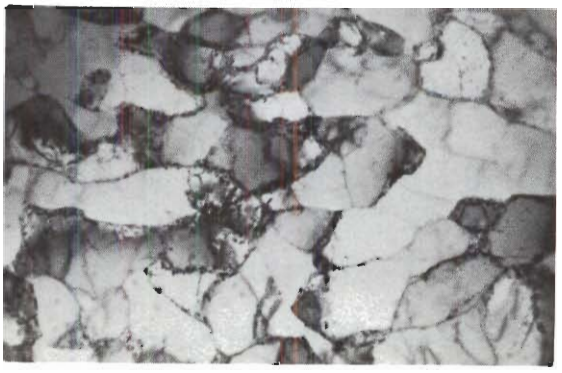

(b)

1μ

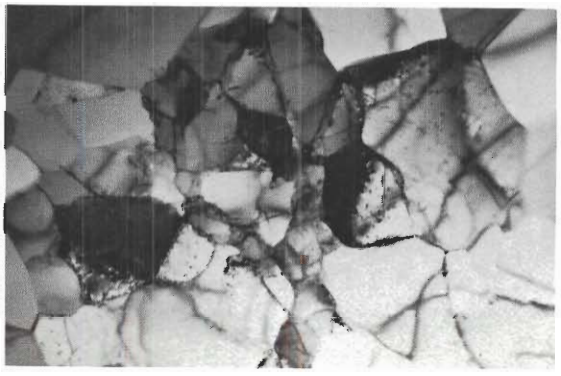

(c)

Figure 5. TEM of Transverse Sections of Cold Drawn Pure Aluminum with Wire Drawing Strains of (a) 0.5, (b) 1.5 and (c) 4.5

(i) and (ii) are related, i.e., they do not vary independently. Steps were taken to evaluate items (ii) and (iii) as they relate to the observed stages of deformation.

Electron diffraction patterns were taken on different samples in the strain range of constant cell size to determine qualitative changes in the misorientation between the cells. It was observed that for strains less than 1.5, cell boundaries were generally low angle while as the strain increased the misorientation between the cells increased substantially to produce high angle boundaries. An example of this behavior is illustrated in Figure 6 where SAD patterns were taken on samples with same cell size but different strains at similar magnification and SAD aperture size. Figure 6(a) taken from a sample with $\varepsilon = 1.47$ shows essentially a single crystal (hkl) pattern. The spots show slight elongations and splitting characteristic of a microstructure consisting of low angle boundaries. Figure 6(b) taken from a sample with $\varepsilon = 4.5$ consists of spotty diffraction rings, characteristic of a polycrystalline structure with high angle boundaries. Since the diffraction patterns were taken on samples of equivalent cell sizes, these results indicate that the strain increases from 1.5 to 4.5 while the cell size remains constant. Selected area diffraction (on individual cells) was used to determine the extent of misorientation between adjacent cells in the high strain region. It was observed that misorientation angles between the cells range from 1 degree to as high as 25 degrees for $\varepsilon > 1.5$. More detailed

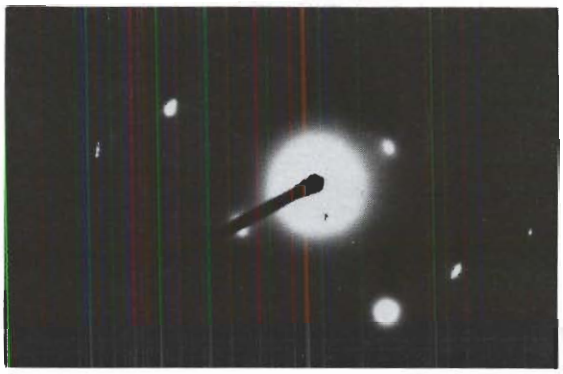

(a)

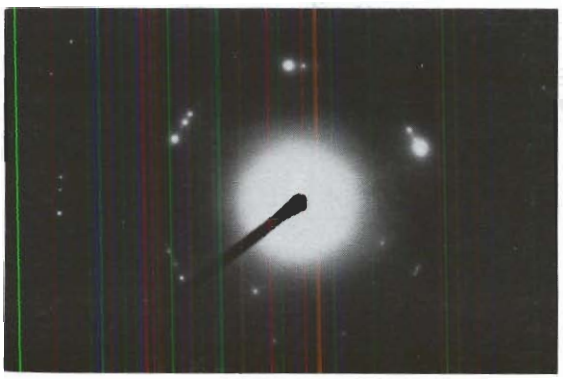

(b)

Figure 6. SAD Patterns of Cold Drawn Pure Aluminum Having L = 0.6μ and True Wire Drawing Strains of (a) 1.5 and (b) 4.5

studies would have to be made to determine the real statistical misorientation distribution and how it changes with strain.

It has been noted that for high temperature deformation of aluminum a steady state (1) is reached where cell size and strength remain constant and the misorientation angles stablize at less than 10 degrees. The present work shows that deformation at room temperature results in contined strengthening and increase in misorientation to high angles while the cell sizes reach a limiting value up to a strain of 4.5. The formation of high angle boundaries during low temperature deformation has previously been reported for Al [9, 12] and for BCC Fe [15].

The possibility that significant changes in the character of the texture might also be important in the strengthening of pure aluminum in high strain region was explored by the use of x-ray transmission pin-hole patterns. A simple <111> fiber texture persists from a strain of 1.5 to 4.5. The patterns show a general sharpening but no variation in the type of texture. This result is not surprising for pure aluminum but should be noted for comparison with the alloy samples in later sections. The sharpening of the texture is consistent with the observed increase in cell misorientation, Young, Anderson and Sherby [23] speculated that in the case of BCC iron the texture influences the substructure but does not contribute directly to the strength. Such a statement can not be verified for aluminum since no attempt was made to determine quantitatively the strengthening component due to texture as an

orientation factor because of the poor reproducibility of the pinhole patterns.

The microstructure and hardening behavior of high purity aluminum during wire drawing at room temperature can be summarized to this point as follows:

1. Rapid strain hardening occurs with initial deformation. The strain hardening diminishes continuously and enters a linear stage at $\varepsilon \simeq 1.5$. Linear hardening continues without saturation to a strain of 4.5. The strain hardening modulus in the linear hardening stage is approximately 1.0 KSI, a very low value in comparison to previously reported vlaues on BCC Fe and FCC Cu.

2. The initial rapid hardening is associated with the formation and refinement of a dislocation cell structure. A recognizable cell structure appears at a strain of 0.3. The cell size decreases continuously (as the strain hardening rate decreases) to $\varepsilon \simeq 1.5$. From this point on the average "cell" size remains constant and subsequent linear hardening is associated with increased boundary misorientation and associated changes in boundary character. There is no consistent Petch-type relationship between yield strength and cell size which is valid over the full range of structures from $\varepsilon = 0.5$ to $\varepsilon = 4.5$.

3. For strains less than 1.5, the cell boundaries are entirely low angle in character. Misorientation angles of the existing cell boundaries increase from a strain of 1.5 to 4.5, ultimately approaching high angle boundaries. In addition some low angle

boundaries continue to form at high strains so that the structure exhibits a duplex boundary character.

4. A single <111> fiber texture develops and continues to sharpen from a strain of 1.5 to 4.5.

Results similar to these have been reported [55] for cold rolled Cu where strengthening increases up to 80% R.A. while the cell sizes stablize after 50% R.A. An important difference should be noted between this behavior and that during heavy wire drawing of BCC Fe [24, 25], where continued cell refinement is associated with linear hardening to true strains of 7.

An approach for correlating structure-property changes during drawing is to systematically fit the tensile stress strain curves obtained at various deformation intervals to the Hollomon equation as described in Chapter II. A non-linear least square curve fitting computer program was used to determine the strengthening coefficient (K) and exponent (n) from equation, $\sigma = K\varepsilon^n$. Figure 7 shows the variation of K and n with wire drawing strains. The values of n range between 0.05 and 0.15 but do not vary systematically. K, however, does vary systematically with strain increasing rapidly up to a strain of 2 and then slowly at higher strains. It should be recalled that cell sizes stablize at higher strains but for strains less than 1.5 the cell sizes decrease as the strain increases. Hence, K appears to be approximately inversly proportional to the cell size up to $\varepsilon = 1.5$ as shown in Figure 8. Morrison [62] observed that for low carbon steels there was extremely weak

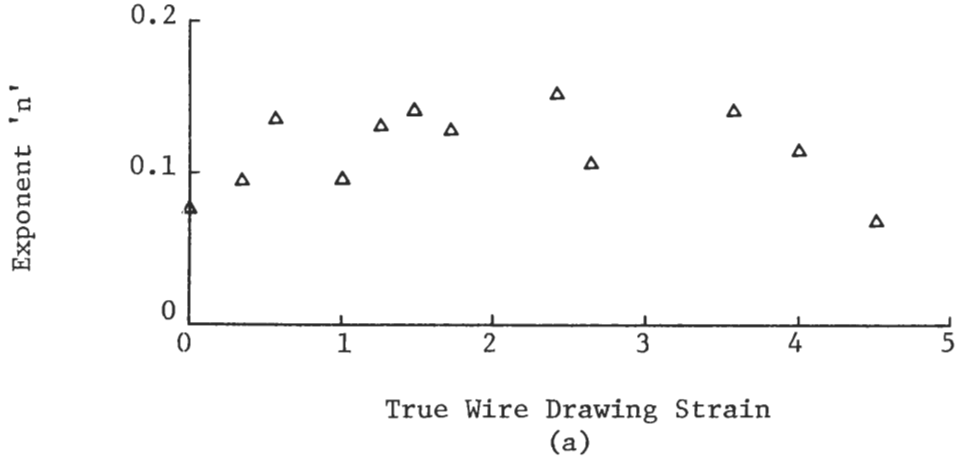

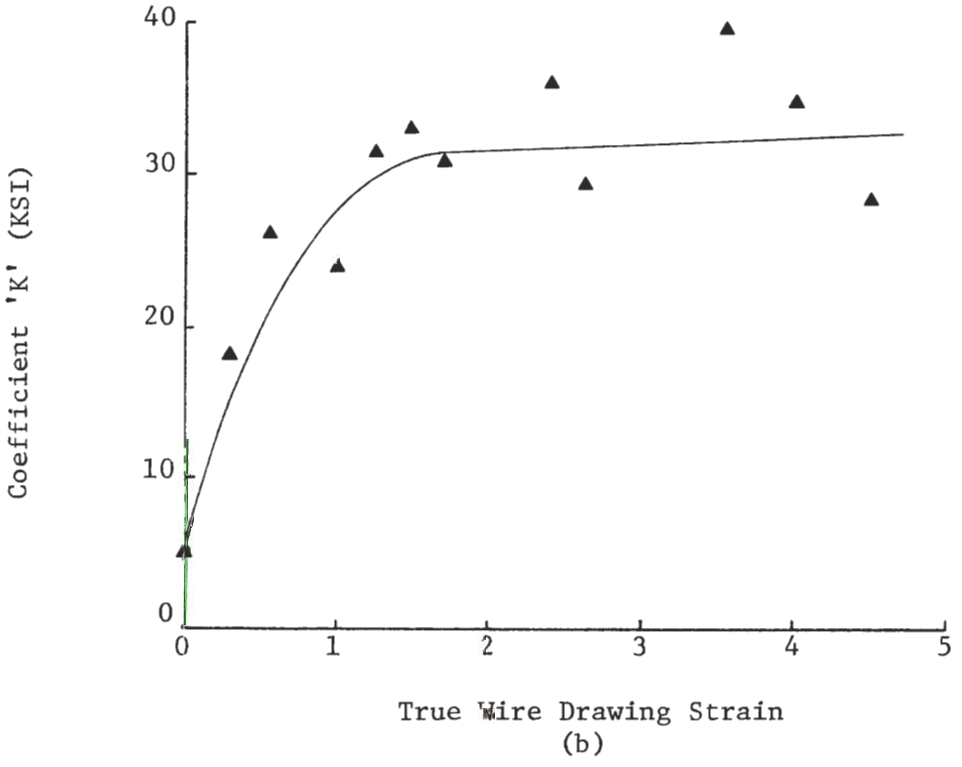

Figure 7. Variation of Strengthening (a) Exponent 'n' and (b) Coefficient 'K' with True Wire Drawing Strains in Cold Drawn Pure Aluminum

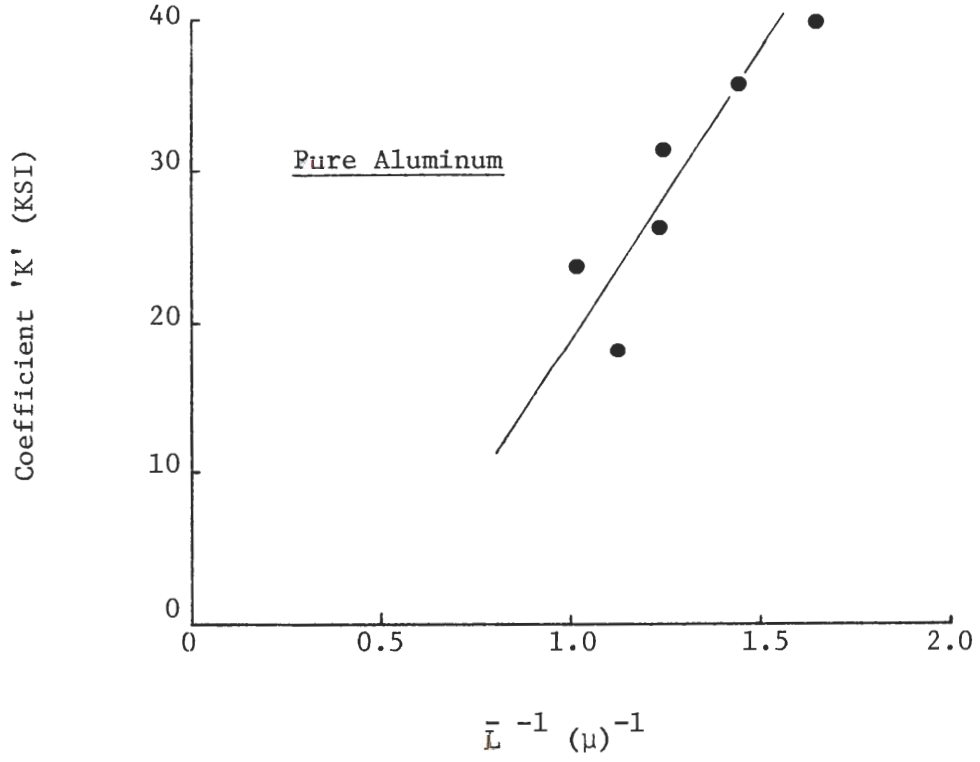

Figure 8. Variation of Strengthening Coefficient 'K' with the Inverse of the Cell Size in Cold Drawn Pure Aluminum

dependency of n on the grain size while a definite inverse proportionality between K and grain size was established. Thus the results obtained in this research indicate that K is mildly structure sensitive up to $\varepsilon = 1.5$ varying approximately inversly with cell size while n is structure insensitive. It must be noted that there are many modifications to the Hollomon equation, as mentioned in literature survey, which may be used for correlating structure-property changes during the drawing for the entire range of wire drawing strains. Only the simplest form of Hollomon equation has been tested in this study.

Cairns et al. [9] have used a similar curve fitting analysis for tensile stress-strain curves from heavily cold rolled Cu. After a reduction of 90% thickness in rolling, dynamic recrystallization was confirmed by TEM. The value of n was found to stablize at 0.59 while the true strain increased from 3 to 5. K values also stablized at slightly less than 90 H Bar from a strain of 3 to 4 and then increases at higher strains.

Al-0.2Mg Alloy

The starting material for this alloy was also a rod of 3/8 inch diameter which had been hot rolled and fully annealed. Figure 9 is an optical micrograph of a longitudinal section showing recrystallized grains. Figure 10 is a TEM micrograph showing the absence of any dislocation cell or subgrain structure in the starting condition.

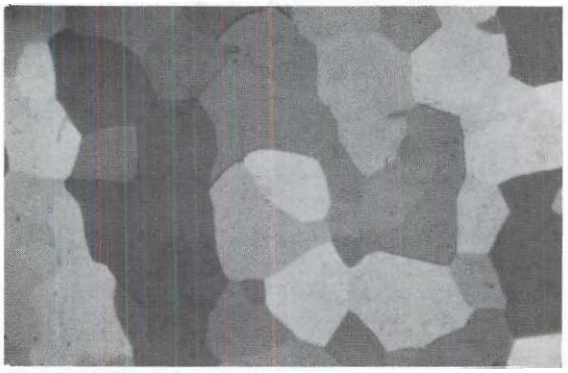

Figure 9. Optical Micrograph of Al-0.2Mg Alloy, Annealed for 3 Hours at 800°F, on its Longitudinal Section

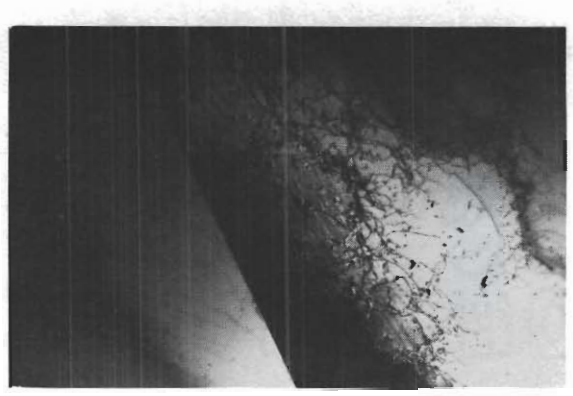

Figure 10. TEM of the Rod of Al-0.2Mg Alloy, Annealed for 3 Hours at 800°F, on its Transverse Section

The strain hardening envelop of this alloy up to a true wire drawing strain of 4.95 is shown in Figure 11. The yield strength increases very rapidly in the initial stages up to a strain of 0.5. Between $\varepsilon = 0.5$ and $\varepsilon = 1.5$ the hardening rate decreases continuously and for strains greater than 1.5 a linear hardening is observed up to a total strain of 4.95. The strain hardening character is generally similar to that of pure aluminum, but the rate is much higher with 0.2% Mg. The strain hardening modulus is 2.28 KSI as opposed to 1.0 KSI for pure aluminum. This value of modulus is still considerably lower than those reported for Fe [25] and Cu [9]. However, it is comparable to an electrical conductor grade aluminum alloy (Al-0.75Fe-0.15Mg) where a value of 2.32 KSI was reported [12]. Since Al-Fe-Mg alloy [12] contains second phase particles (stable $FeAl_3$ and unstable $FeAl_6$) and 0.2% Mg is completely soluble in aluminum, it seems that value of modulus is not affected appreciably by the presence of small amounts of the iron-rich precipitate. This kind of observation has also been made for BCC iron where Rack and Cohen [24] have shown that additions of 3.16% Ti (containing Fe_2Ti particles) and 1.08% Ti (in substitutional solid solution with Fe) do not change the strain hardening modulus of Fe in wire drawing at large strains. Thus, this value of modulus is not affected by the soluble and insoluble additions of alloying elements in BCC iron while in pure aluminum it is clearly affected by small amounts of soluble additions.

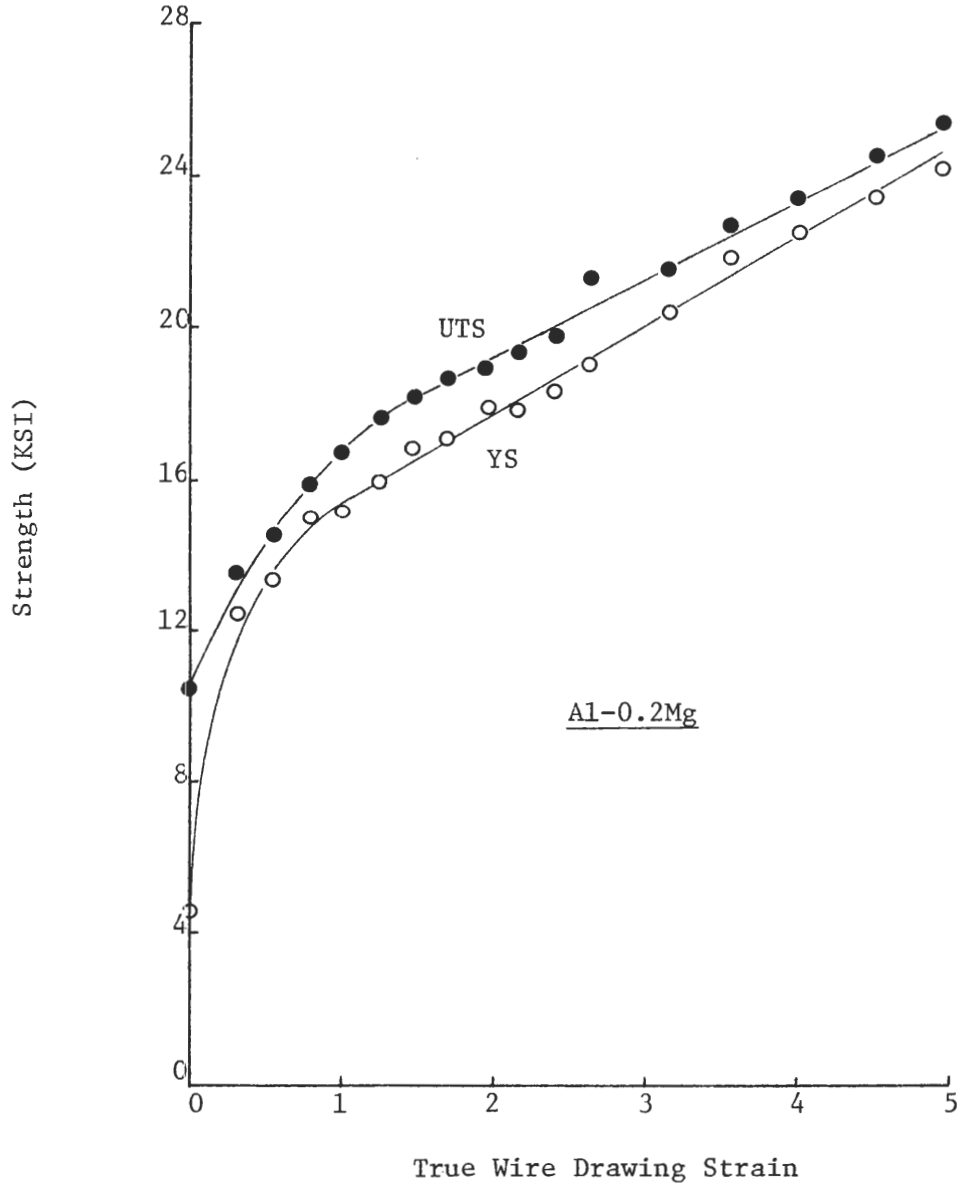

Figure 11. Strain Hardening Envelop of Cold Drawn Al-0.2Mg Alloy

The variations in cell sizes in Al-0.2Mg up to strains of 4.95 (determined by TEM) is shown in Figure 12. Cell formation was noted at an earlier stage than for pure aluminum ($\varepsilon = 0.3$ vs. $\varepsilon = 0.5$) and the cell sizes were smaller at equivalent strains up to $\varepsilon = 1.5$. This indicates that small amounts of Mg in solid solution with Al enhances the process of cell size formation and refinement. This observation is contrary to that made by McElroy and Szkopiak (1). These authors concluded that solute atoms in solid solution delay the formation of dislocation tangles and cells to higher strains in the deformation process.

Cell refinement continued in Al-0.2Mg to a strain of $\simeq 1.5$ and $\bar{L} \simeq 0.5$. From this point the cell size began to increase and continued to do so at a gradual but decreasing rate to $\varepsilon = 4.95$. This behavior differs from pure Al where the average cell size was found to remain constant in the high strain region. Micrographs showing the cell boundary character at various stages ($\varepsilon = 0.3$, 1.5 and 4.95) are shown in Figure 13. The general behavior is similar to that of pure Al in that a general trend toward sharper boundaries and cleaner "cells" accompanied higher strains. There is a major difference in the degree of the trend however. In Al-Mg the cells after $\varepsilon \simeq 1.5$ showed much sharper boundaries and were more free of internal dislocations and shows smaller minimum cell size compared to pure aluminum.

Electron diffraction patterns were taken on different samples over the entire range of wire drawing strains to determine qualitative

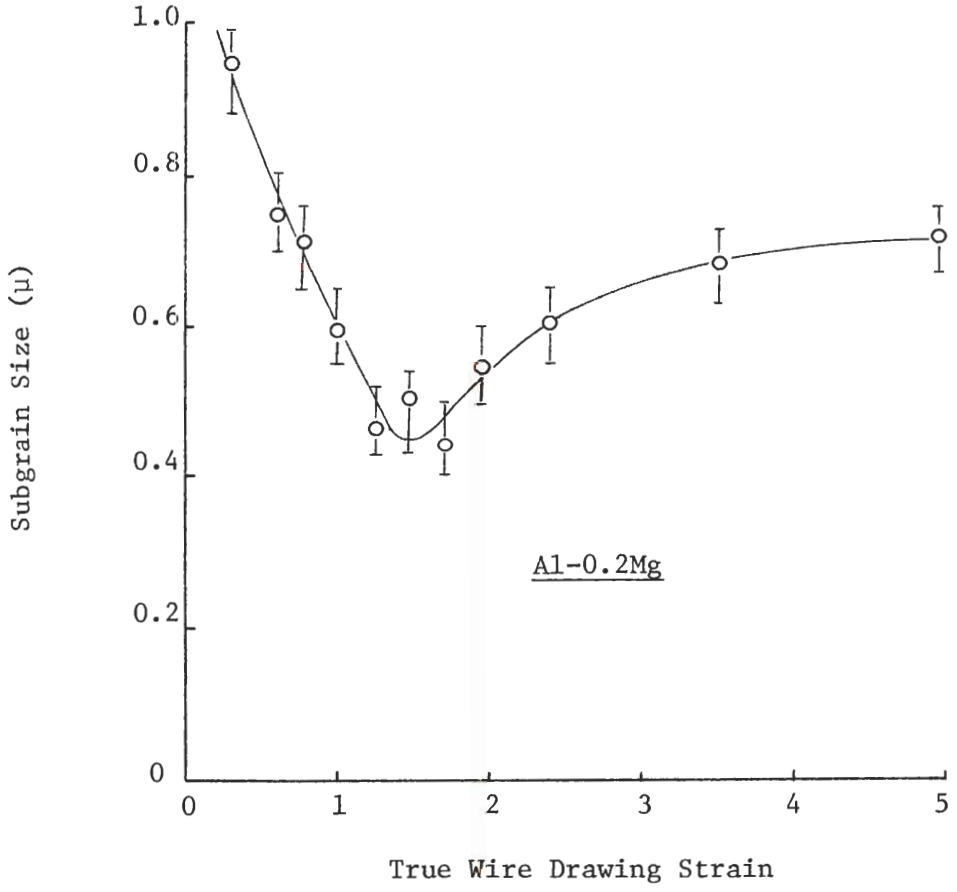

Figure 12. Variation of Cell Size as a Function of True Wire Drawing Strain in Al-0.2Mg Alloy

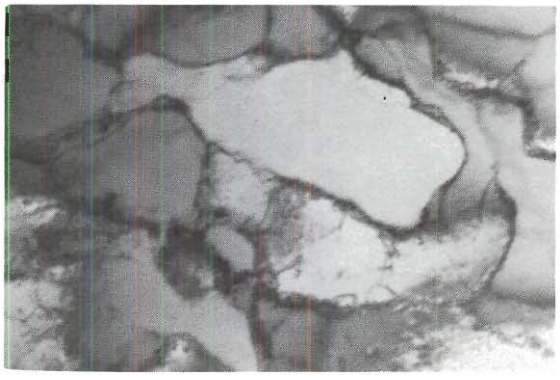

(a)

(b)

1μ

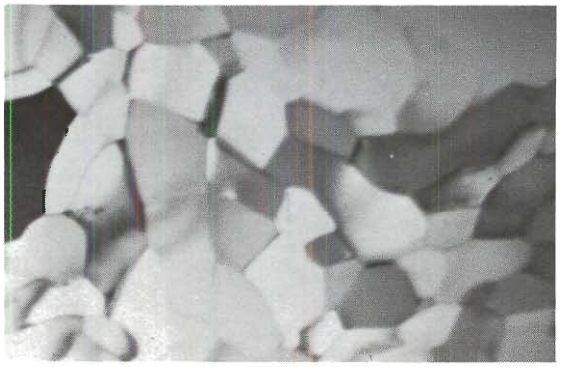

(c)

Figure 13. TEM of Transverse Sections of Cold Drawn Al-0.2Mg Alloy with Wire Drawing Strains of (a) 0.3, (b) 1.5 and (c) 4.95

changes in misorientation between the cells. In the range of decreasing cell size it was observed that cell boundaries were generally low angle while as the cell size increased the misorientation between cells increased substantially to produce high angle boundaries. An example of this behavior is shown in Figure 14 where SAD patterns were taken on samples with same cell size but different strains at similar magnification and SAD aperture size (same procedure used for pure aluminum). Figure 14 shows that for $\varepsilon = 0.774$ the SAD pattern consists of spots slightly elongated and splitted which is characteristic of a microstructure consisting of low angle boundaries. For $\varepsilon = 4.5$, SAD pattern consists of spotty diffraction rings which is characteristic of polycrystalline structure with high angle boundaries. Thus it was concluded that misorientation angles of the cells increase from a strain of 1.5 to 4.95 in Al-0.2Mg alloy, an observation similar to that was made for pure aluminum earlier. SAD on individual cells was used to determine the extent of misorientations between the adjacent cells in the range of increasing cell size. It was observed that misorientation angles between cells range from 1° to as high as 25° in this alloy also for $\varepsilon > 1.5$. The trend of sharpening boundary character and increasing average "cell" size together with the observed high angle boundaries indicates a region of dynamic low temperature (DLT) recrystallization at $\varepsilon > 1.5$.

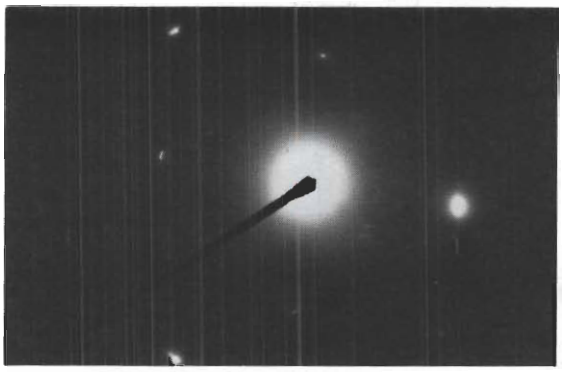

(a)

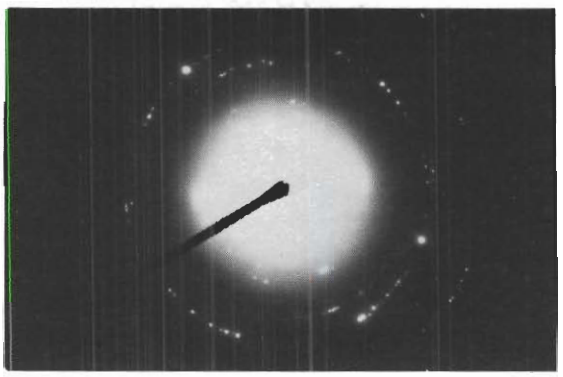

(b)

Figure 14. SAD Patterns of Cold Drawn Al-0.2Mg Alloy Having $\bar{L}$ = 0.72μ and True Wire Drawing Strains of (a) 0.77 and (b) 4.5

The character of the texture for the Al-Mg alloy was explored by the use of x-ray transmission pinhole patterns. A simple <111> fiber texture was found to persist to high strains with sharpening being the only variation. This result should be compared to the duplex <111> <100> fiber texture found in cold-drawn Al-0.9Mg alloy at ε 2.8 [27]. It is interesting that if the difference in composition of 0.6% Mg can produce such a difference in results.

The microstructure and hardening behavior of Al-0.2Mg alloy during wire drawing at room temperature can be summarized to this point as follows:

1. The characteristics of the strain hardening envelop are similar to the one observed for pure aluminum indicating that shape of the strain hardening envelop is not altered by the addition of 0.2% Mg in solid solution. The linear hardening continues without saturation to a strain of 4.95. The hardening modulus in the linear hardening region is 2.28 KSI compared to 1.0 KSI observed for pure aluminum, still quite low when compared with previously reported values on BCC Fe and FCC Cu.

2. The initial rapid hardening is associated with the formation and refinement of a dislocation cell structure. A recognizable cell structure is seen at $\varepsilon = 0.3$ compared to $\varepsilon = 0.5$ for pure aluminum. The cell size decreases continuously up to $\varepsilon = 1.5$ as the strain hardening rate decreases. From this point on the cell size increases while the alloy continues

to harden up to an $\varepsilon = 4.95$. There is no consistent Hall-Petch type relationship between yield strength and cell size valid over the full range of structures from $\varepsilon = 0.3$ to $\varepsilon = 4.95$.

3. The misorientation angles of the cells remain low up to a strain of 1.5 and it increases considerably from a strain of 1.5 to 4.95, ultimately approaching high angle boundaries.

4. A single <111> fiber texture develops and continues to sharpen from a strain of 1.5 to 4.95. There is no evidence of the existence of a duplex texture.

The strengthening coefficients (K) and exponents (n) were calculated from tensile stress-strain curves of the wires selected at different stages in the wire drawing reduction sequence (see pure aluminum section for details) of this alloy. Figure 15 shows the variation of K and n with wire drawing strains. The values of n range from 0.05 to 0.15 but do not vary systematically. However, K increases from 5 to 36 KSI up to a strain of 2.0 and for strains greater than 2.0 it increases slowly to 38.5 KSI up to a total strain of 4.95. It should be noted that "cell" sizes start to increase after a strain of 1.5. Below $\varepsilon = 1.5$ the cell size decreases which suggests an inverse proportionality between K and cell size and is shown in Figure 16. Thus in this alloy also, similar to pure aluminum, K is found to be mildly structure sensitive and to vary inversely with average "cell" size for $\varepsilon < 1.5$ while n shows no consistent structural dependence.

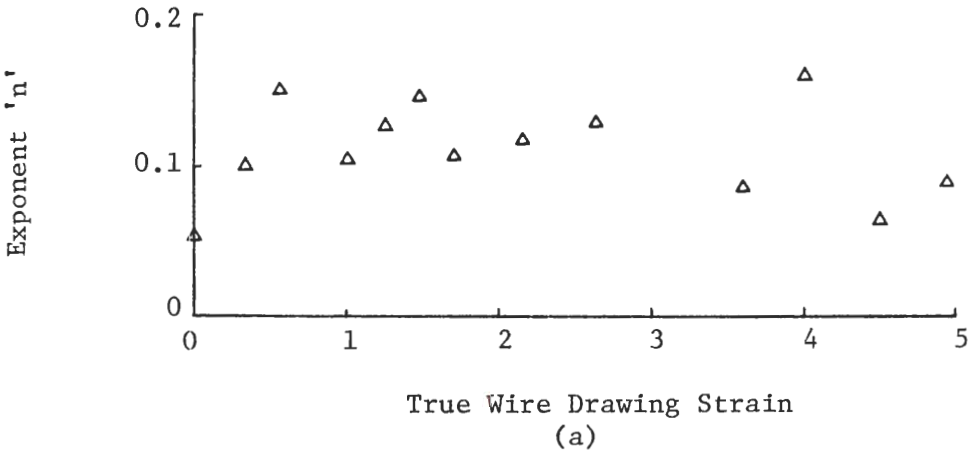

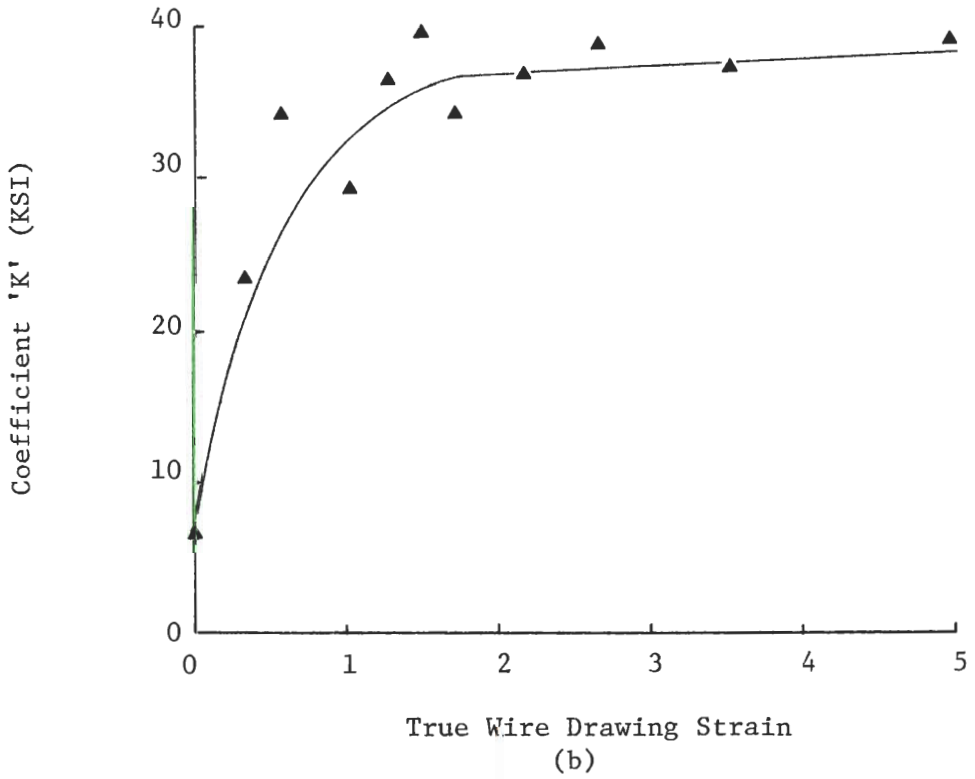

Figure 15. Variation of Strengthening (a) Exponent 'n' and (b) Coefficient 'K' with True Wire Drawing Strains in Cold Drawn Al-0.2Mg Alloy

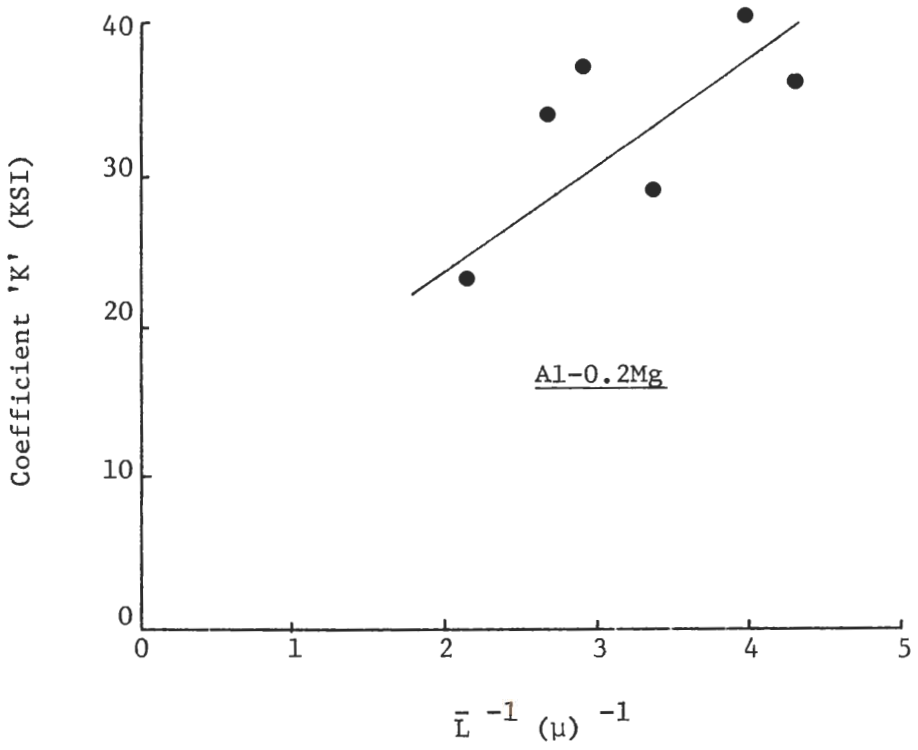

Figure 16. Variation of Strengthening Coefficient 'K' with the Inverse of the Cell Size in Cold Drawn Al-0.2Mg alloy

Al-0.6Fe Alloy

Iron was selected an an insoluble alloying element in order to study the effect of small amounts of precipitates on the strain hardening behavior of dilute Al alloys during wire drawing. Figures 17 and 18 show the microstructure of the starting hot rolled and recrystallized 3/8 inch rod. It is a fully recrystallized structure with small amounts of $FeAl_3$ precipitates characteristically distributed at grain boundaries [58].

The strain hardening envelop of this alloy up to a true strain of 4.95 is shown in Figure 19. The yield strength initially increases rapidly up to a strain of 0.5. From a strain of 0.5 to 2.2 the hardening rate decreases and is followed by work softening up to a final strain of 4.95. It should be recalled that in pure aluminum and Al-0.2Mg alloy linear hardening was observed between the strains of 1.5 and 4.5. The initial hardening in this alloy up to a strain of 1.5 is nearly 13 KSI compared to 10 KSI for pure aluminum and 12 KSI for Al-0.2Mg alloy. The strain hardening envelop exhibited here is typical of materials showing dynamic recrystallization. Nutting [27] has reported such curves for OFHC Cu and Al where work softening due to dynamic recrystallization in cold rolling after strains of 3.0 and 3.5 respectively was observed.

A distinct cell structure is observed in Al-0.6Fe at $\varepsilon = 0.3$. The variations in cell sizes over the entire strain range up

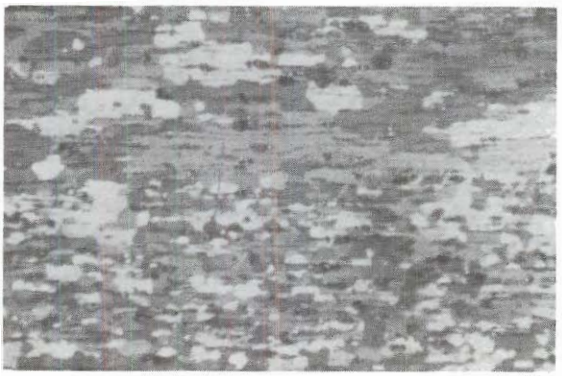

Figure 17. Optical Micrograph of Al-0.6Fe Alloy, Annealed for 3 Hours at 800°F, on its Longitudinal Section X40

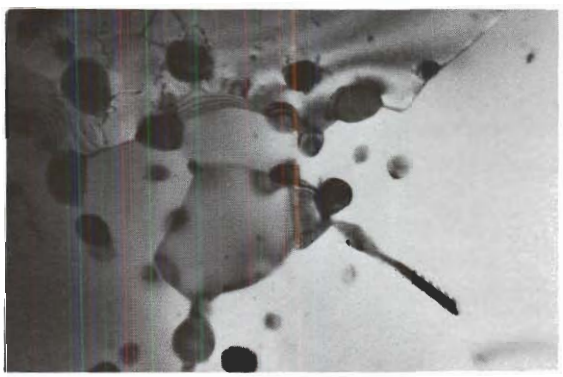

Figure 18. TEM of Al-0.6Fe Alloy, Annealed for 3 Hours at 800°F, on its Transverse Section

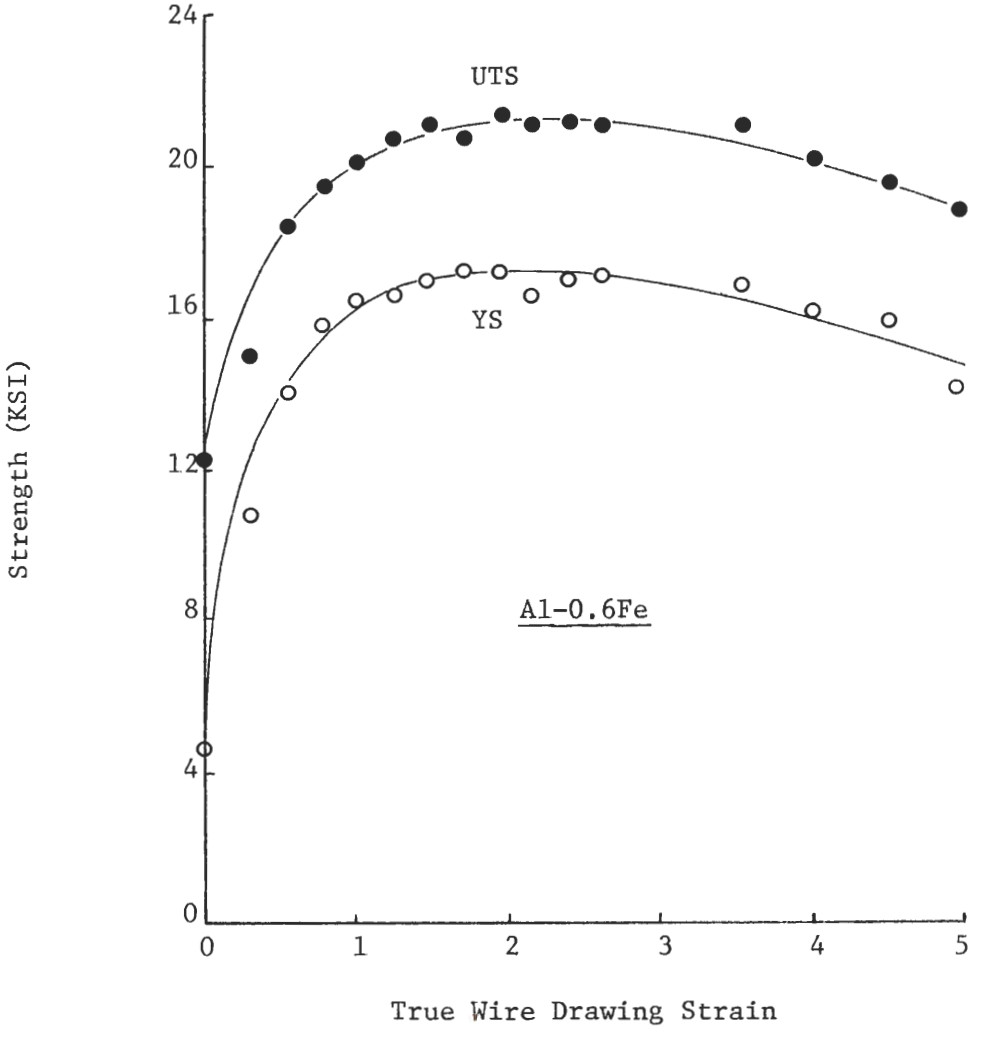

Figure 19. Strain Hardening Envelop of Cold Drawn Al-0.6Fe Alloy

to 4.95 is shown in Figure 20. Between 0.3 and $\simeq$ 2.5 the size decreases with increasing strain. For comparison, in pure aluminum and Al-0.2Mg alloy distinct cell structures were detected at ε = 0.5 and 0.3 respectively and cell size refinement was observed only up to a strain of 1.5 in each case. The magnitudes of cell sizes in Al-Fe are consistently lower than for pure aluminum at equivalent strains and approximately equal to that of Al-Mg. The minimum cell size in Al-Fe is approximately 0.35μ as opposed to 0.6μ for Al and 0.45μ for Al-Mg. From ε = 2.5 to 4.95 there is general increase in average cell size for the Al-0.6Fe alloy.

The character of the "cell" structure at various intervals is shown in Figure 21. There is a general sharpening of boundaries with increasing strain. In the growth region $2.5<\varepsilon<4.95$ the "cells" are equiaxed and have very sharp boundaries reminescent of grains. The interiors are relatively free of dislocations. The cell size distribution during growth appeared to be uniform.

Selected area electron diffraction patterns were taken according to procedures previously described to qualitatively evaluate the boundary misorientation. Examples are shown in Figure 22. These types of patterns and SAD analysis of individual cells clearly indicate that for $\varepsilon < 2.5$ the boundary character is low angle and for $\varepsilon > 2.5$ it is predominantly high angle in character. The region of increasing "cell" size ($\varepsilon > 2.5$) is one of DLT recrystallization similar to that observed in Al and Al-Mg.

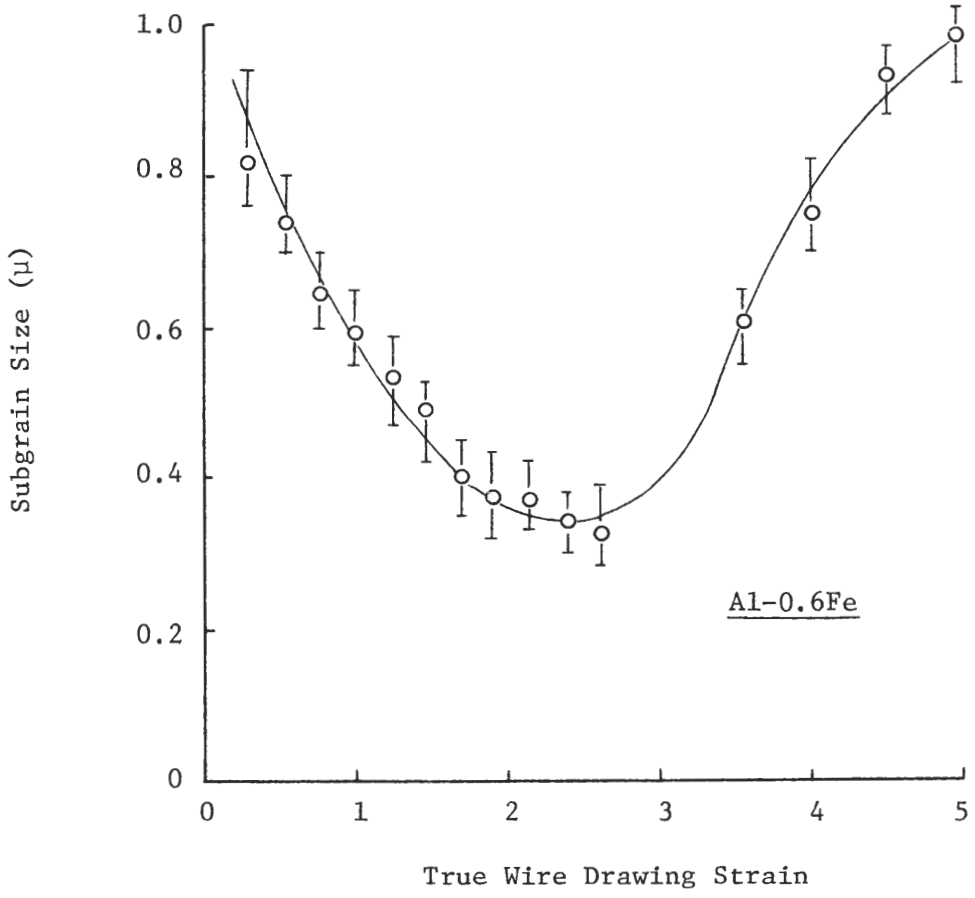

Figure 20. Variation of Cell Size as a Function of True Wire Drawing Strain in Al-0.6Fe Alloy

(a)

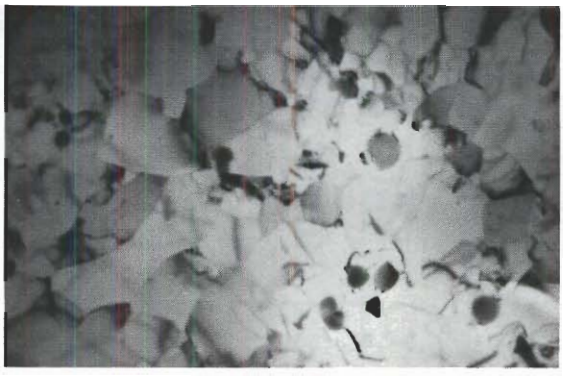

(b)

(c)

Figure 21. TEM of Transverse Sections of Cold Drawn Al-0.6Fe Alloy with Wire Drawing Strains of (a) 0.3, (b) 1.5 and (c) 4.95

(a)

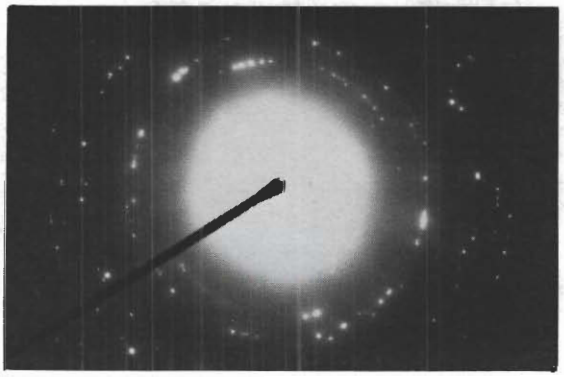

(b)

Figure 22. SAD Patterns of Cold Drawn Al-0.6Fe Alloy Having $\bar{L}$ = 0.6μ and True Wire Drawing Strains of (a) 1.0 and (b) 3.56

Qualitative measurements of preferred orientation were obtained by x-ray pinhole patterns. These showed a simple <111> fiber texture which sharpened with strain but did not change in character up to $\varepsilon = 4.95$.

Thus two distinct stages can be seen from the comparison of strain hardening and cell size curves in Al-0.6Fe. The increase in "cell" size and decrease in strength for $\varepsilon > 2.5$ and 2.2 respectively is attributed to the process of DLT recrystallization which may be enhanced by the distribution of $FeAl_3$ precipitates. Chia and Starke [58] have shown that annealing the rod after hot rolling (which is the case here) washes out some of the microstructural features which enhances a uniform distribution of precipitates during later processing. The non-uniform distribution of precipitates can lead to dynamic recrystallization during deformation since these precipitates can act as nucleation centers. In the present work the initial precipitate distribution was non-uniform; however, it had become quite uniform by the time strains reached the DLTR stage. Consequently cell growth during the DLTR stage was uniform and no anomalously large nuclei were seen. Delaying of the recrystallization stage by going to low deformation temperatures apparently allows for further homogenization of the structure and a more uniform growth during the recrystallization stage.

The microstructure and hardening behavior of Al-0.6Fe during wire drawing at room temperature can be summarized as

follows:

1. Rapid strain hardening occurs with initial deformation up to $\varepsilon = 0.3$. The strain hardening diminishes up to $\varepsilon = 2.2$ and work softening occurs for $\varepsilon > 2.2$.

2. The initial rapid work hardening is associated with the formation and refinement of a dislocation cell structure. A recognizable cell structure is seen at $\varepsilon = 0.3$ compared to pure aluminum where distinct cell structure appeared at $\varepsilon = 0.5$ only. The average cell size decreases continuously as the hardening rate decreases to $\varepsilon = 2.5$. From this point on the cell size increases and work softening is associated with increased boundary misorientation.

3. For $\varepsilon < 2.5$, the cell boundaries are entirely low angle in character while it seems to be increasing substantially for $\varepsilon > 2.5$ producing high angle boundaries. Uniform coarsening of the cells occurs during dynamic recrystallization. Nucleation could not be observed.

4. A weak single <111> fiber texture persists up to $\varepsilon = 2.6$ and no variation in the type of texture was observed over the whole range of strains from $\varepsilon = 0.3$ to $\varepsilon = 4.55$.

The variations of strengthening coefficient (K) and exponent (n) determined from tensile stress-strain curves (see pure aluminum section for details) are shown in Figure 23. The values of n range from 0.10 to 0.20 as compared to values of 0.05 to 0.15 observed for pure aluminum and Al-0.2Mg alloys. The values

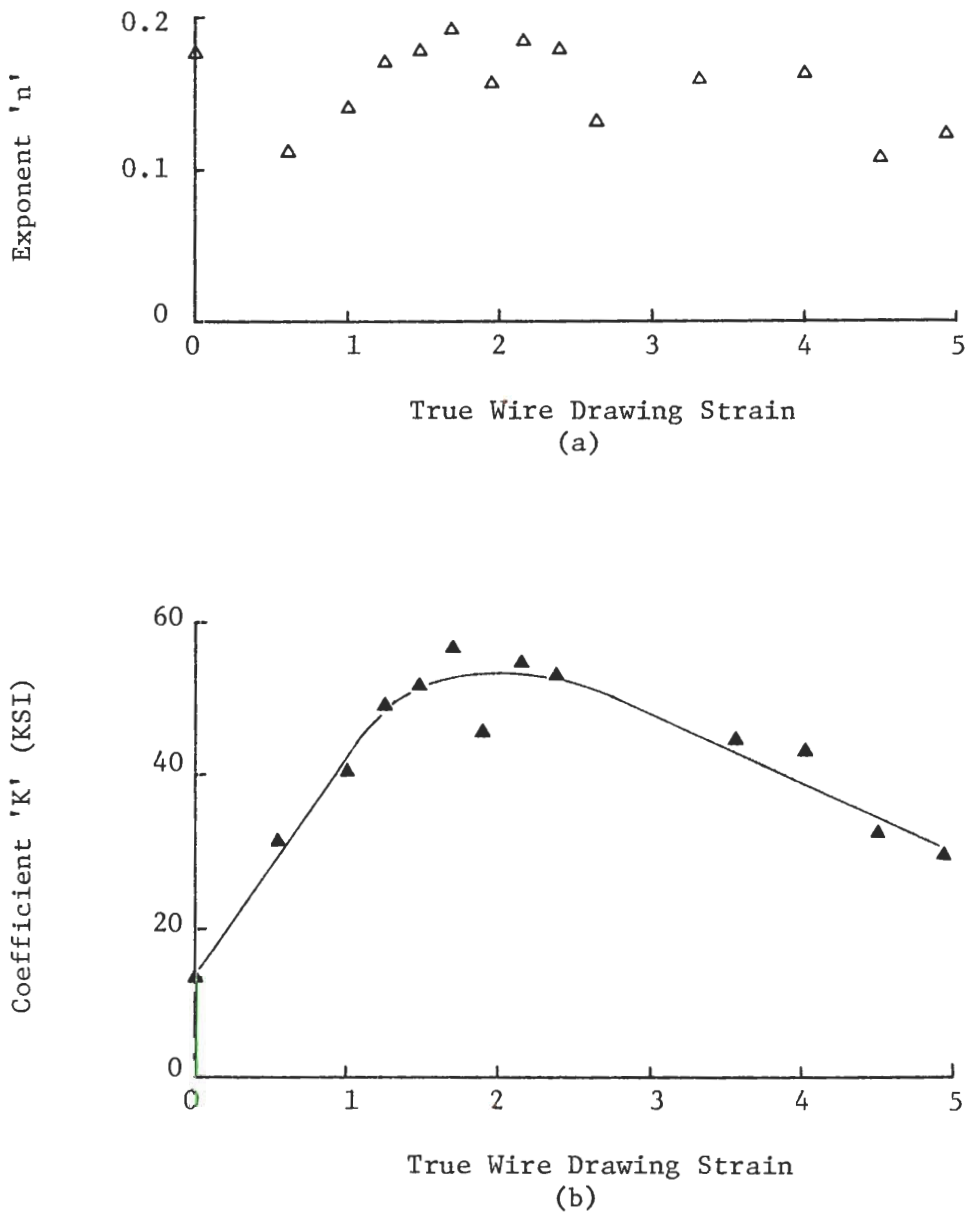

Figure 23. Variation of Strengthening (a) Exponent 'n' and (b) Coefficient 'K' with True Wire Drawing Strains in Cold Drawn Al-0.6Fe Alloy

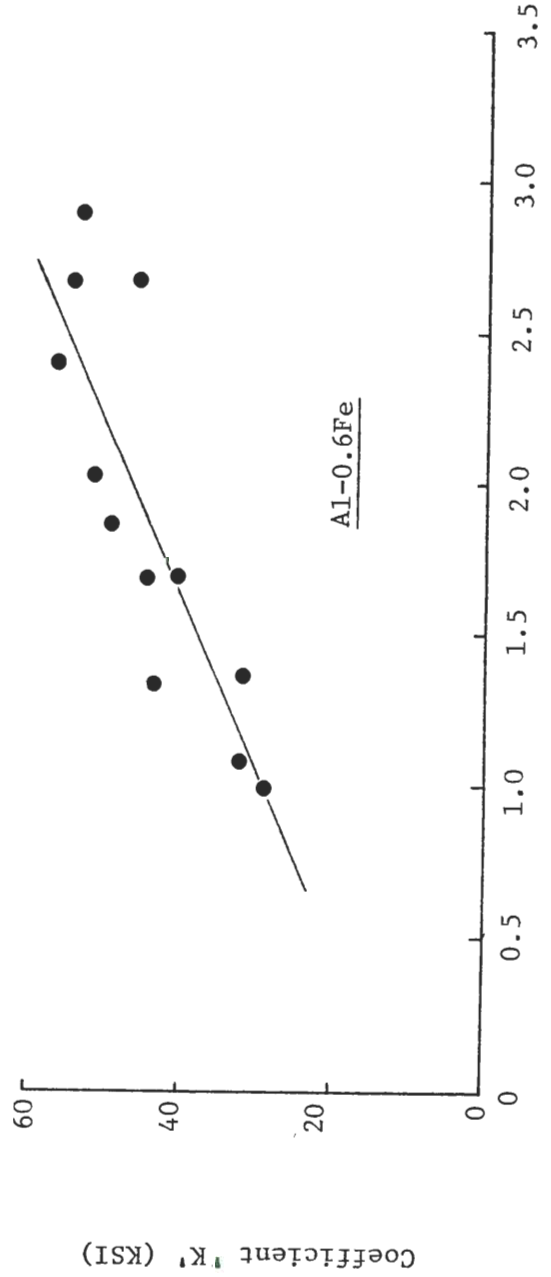

Figure 24. Variation of Strengthening Coefficient 'K' with the Inverse of the Cell Size in Cold Drawn Al-0.6Fe Alloy

of n do not vary systematically. However, K increases from 13 to 53 KSI up to a strain of nearly 2 and decreases to 30 KSI at $\varepsilon = 4.95$. The inverse proportionality between K and cell size has been found to be excellent in this alloy as shown in Figure 24. Thus in this alloy also K is found to be quite structure sensitive while n remains structure insensitive.

EC Aluminum

The starting material for EC aluminum was also a rod of 3/8 inch diameter in a fully annealed condition. The strain hardening envelop of EC aluminum when it is subjected to a wire drawing strain of 4.95 (this strain corresponds to a wire diameter of 0.032 inch) as shown in Figure 25. The yield strength increases rapidly in the initial stage of strain hardening. Between strains of 0.5 and 1.5 the hardening rate decreases and for $\varepsilon > 1.5$ a linear hardening is observed up to total strain of 4.95. The strain hardening modulus in the high strain range is 2.16 KSI as compared to pure aluminum and Al-0.2Mg alloy where values of 1.0 and 2.28 KSI were observed. EC aluminum which contains nominally 0.075% Fe and 0.05% Si seems to affect the strain hardening modulus similar to Al-0.2Mg alloy since the value of modulus in the two cases is observed to be essentially the same. As mentioned in the pure aluminum section the presence of small quantities of impurites can affect the modulus of pure aluminum considerably. It should also

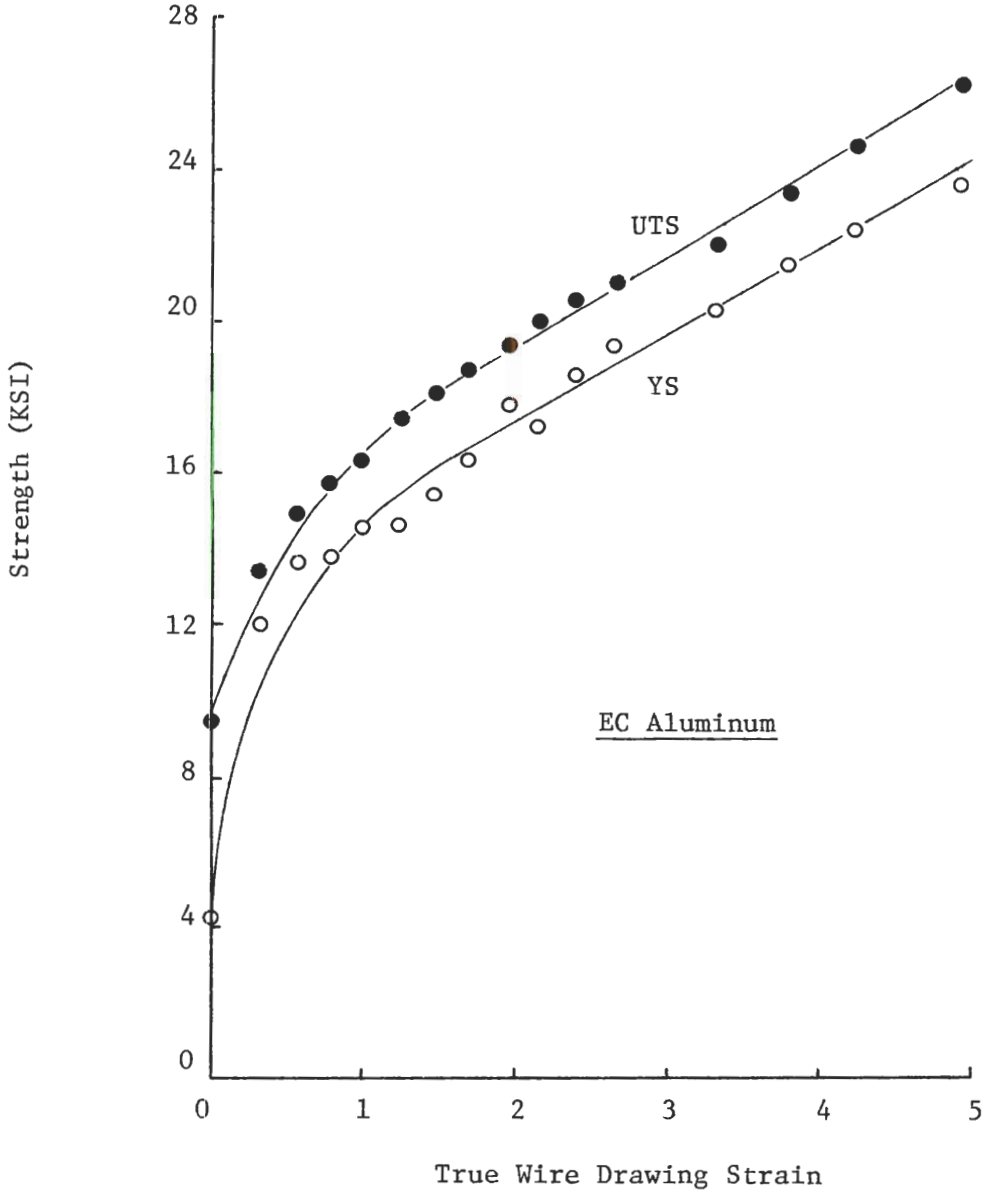

Figure 25. Strain Hardening Envelop of Cold Drawn EC Aluminum

be noted that amount of alloying additions in the range of conductor grade aluminum does not seem to change the strain hardening modulus to any appreciable extent (for both soluble and insoluble additions).

The variation of cell sizes observed by TEM with wire drawing is shown in Figure 26. A distinct cell structure was observable by TEM only after an $\varepsilon = 0.5$ similar to pure aluminum. Between strains of 0.5 and 2.6 the cell size decreases with increasing strain. The magnitudes of cell sizes in this alloy are comparable to Al-0.6Fe alloy. The minimum cell size observed in this alloy was 0.25μ as opposed to 0.35μ in Al-0.6Fe alloy. After a strain of 2.6 (DLTR region), the cell size suddenly increases to a value of 0.5μ and stablizes at this cell size up to $\varepsilon = 4.95$. Figure 27 shows the cell structure characteristic of these strains. Along with the decreasing cell size there is a sharpening of the cell boundaries with increasing strain. At $\varepsilon = 4.95$ the cell structure consists of equiaxed cells almost void of internal dislocations. It indicates that EC aluminum has undergone considerable polygonization after an $\varepsilon = 2.6$.

The misorientation angles of the cells in EC aluminum were determined qualitatively by taking SAD patterns on different samples. The conditions under which these patterns were taken are described in pure aluminum section. The results of the study of misorientation angles of cells in this alloy indicate

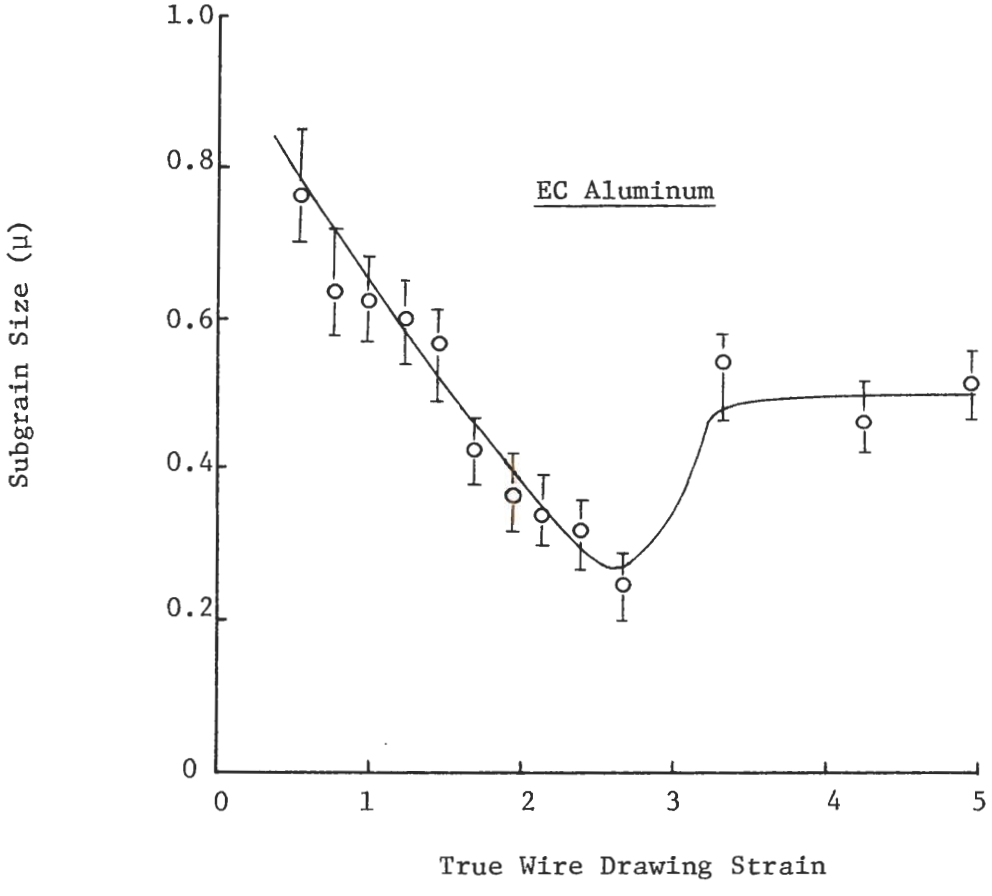

Figure 26. Variation of Cell Size as a Function of True Wire Drawing Strain in EC Aluminum

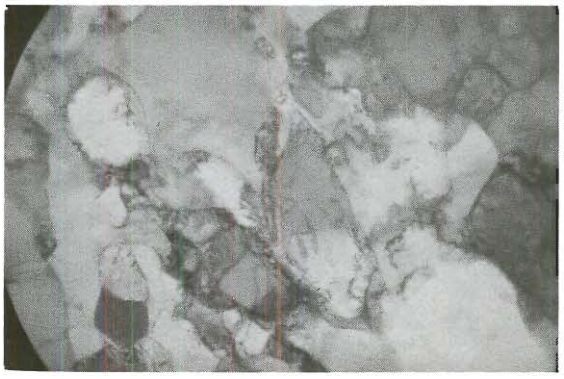

(a)

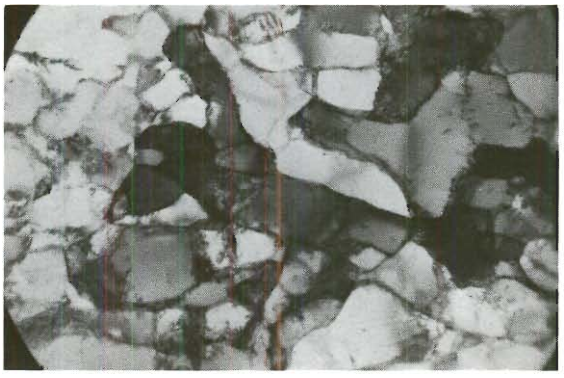

(b)

Figure 27. TEM of Transverse Sections of Cold Drawn EC Aluminum with Wire Drawing Strains of (a) 0.5, (b) 1.5, (c) 2.6 and (d) 4.95

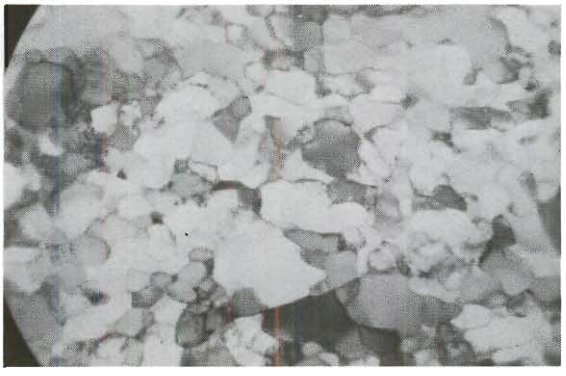

(c)

١٣

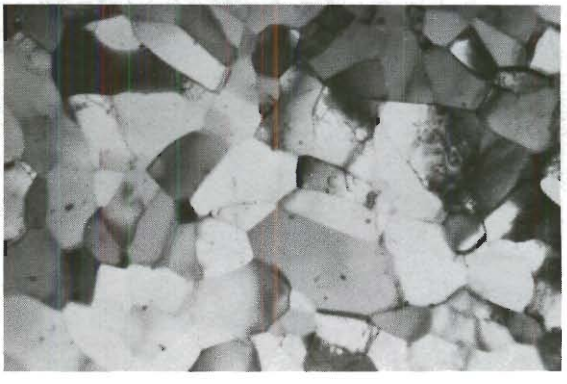

(d)

that the microstructure consists of low angle cell boundaries up to an $\varepsilon = 2.6$ while the stablization of the cell size for $\varepsilon > 2.6$ is accompanied by increase in misorientation angles of the cells. An example of this behavior is illustrated in Figure 28. The increase in misorientation angles of the cells is clearly seen in the sample with $\varepsilon = 3.3$ where spotty diffraction rings which are characteristic of a polycrystalline structure containing high angle boundaries. Thus it is speculated that the contribution of increase in cellular misorientation angles to the strengthening of this alloy in DLTR region is similar to pure aluminum. An interesting observation that can be made from the study of the variation of cellular misorientation angles in all the four materials is that cells consist of low angle boundaries as long as its refinement occurs. This point will be discussed later in general discussion section.

The use of x-ray transmission pinhole patterns on different samples of EC aluminum also indicate that a single <111> fiber texture persists in DLTR region. These patterns show that there is general sharpening but no change in the type of texture. Thus it is concluded that texture is also perhaps contributing to the strength in the strain range of constant cell size.

The results obtained by deforming EC aluminum in wire drawing up to a strain of 4.95 can be summarized as follows:

1. There is a rapid strain hardening up to $\varepsilon = 0.5$. Between strains of 0.5 to 1.5 the hardening rate diminishes

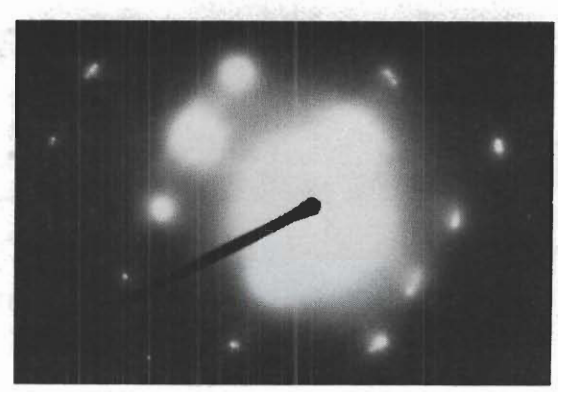

(a)

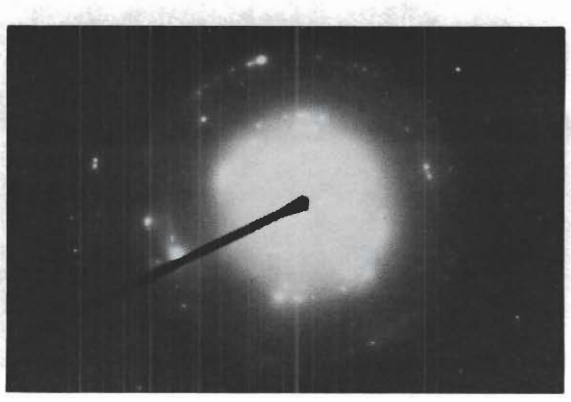

(b)

Figure 28. SAD Patterns of Cold Drawn EC Aluminum Having $\bar{L}$ = 0.55μ as True Wire Drawing Strains of (a) 1.25 and (b) 3.3

continuously and enters a linear stage. The linear hardening persists up to $\varepsilon = 4.95$. The strain hardening modulus in linear hardening range is 2.16 which is nearly the same which was observed for Al-0.2Mg alloy (2.28 KSI).

2. The initial rapid hardening is associated with the formation and refinement of dislocation cell structure. A recognizable cell is seen at $\varepsilon \simeq 0.5$. The average cell size decreases as the strain hardening increases to an $\varepsilon = 2.6$, for $\varepsilon > 2.6$, the cell size suddenly increases and stablizes at a value of 0.5μ. The subsequent hardening is associated with increase in cell misorientation angles and texture in the DLTR region. There is no consistent Petch-type relationship between yield strength and cell size which is valid over the full range of structures from 0.5 to 4.95.

3. The microstructure consists of cell boundaries low angle in character up to a strain of 2.6. Misorientation of the cells increases in the DLTR region, ultimately approaching high angle boundaries.

4. A single <111> fiber texture develops and continues to sharpen from a strain of 2.6 to 4.95.

General Discussion

It is now possible to summarize the important characteristics of strain hardening and microstructure development during low temperature wire drawing of the dilute aluminum alloys used

in this study. Starting with the recrystallized rod, very rapid strengthening occurs up to a strain of 0.5 and then continues at a diminishing rate from $\varepsilon = 0.5$ to $\varepsilon = 1.5$. The absolute values of strength levels and the strain hardening rates differ with the alloying additions. Linear hardening begins at $\varepsilon \simeq 1.5$ and continues to $\varepsilon \simeq 5$ in pure aluminum, Al-0.2Mg and EC aluminum. In Al-0.6Fe alloy work softening occurs after a strain of 2.2 (hardening rate decreases continuously up to an $\varepsilon = 2.2$ in this alloy). Soluble additions have a great effect on the linear hardening region as characterized by its hardening modulus. This value for pure aluminum was 1.0 KSI while for EC aluminum and Al-0.2Mg alloy the values were 2.6 and 2.28 KSI. These values compare favorably with others reported in the literature for conductor grade Al-Fe-Mg alloy [12]. However the modulii observed in the aluminum alloys of this study are extremely low when compared with Fe [25] and Cu [9] where values of 20.5 and 7.5 KSI were reported. In Fe, it was also observed that values of modulii were not affected by the presence of soluble and insoluble additions of alloying elements [24]. The distinct work softening in Al-0.6Fe alloy observed here is similar to the results obtained for pure Cu and Al [27]. These authors found that softening in Cu and Al during cold rolling occurs at strains of 3.0 and 3.5 respectively.

Microstructural developments are characterized by different stages in the deformation process. Distinct cell structures

were observable at a strain of 0.5 in pure and EC aluminum and at 0.3 in Al-0.2Mg and Al-0.6Fe alloys (will now be referred to as stage I). Stage I consists of multiplication of dislocations and formation of dislocation tangles which ultimately results in the appearance of a distinct cell structure. The results indicate that presence of alloying elements decreases the minumum strain necessary to produce a distinct cell structure. The lowering of the SFE as a result of alloying can create back stress, by pinning solute atoms, which can force some of the dislocations to cross slip and promote the appearance of a distinct cell structure to a smaller strain during wire drawing of alloys [74]. The next stage (stage II) is characterized by the formation of low angle cell boundaries and their refinement. In pure aluminum and Al-0.2Mg alloy, this stage extends to a strain of 1.5 while in EC aluminum and Al-0.6Fe alloy stage II can extend as far as $\varepsilon = 2.6$ with lower minimum cell sizes. The cell structure consists of ragged boundaries which are refined continually as the strain increases. The character of the boundaries remain low angle. In stage III, dynamic low temperature recrystallization (DLTR) results in the formation of high angle boundaries. In this region the "cells" consist of a mixture of dislocation cell boundaries (low angle), subgrain boundaries (low angle) and grain boundaries (high angle). The average size depends on the competitive mechanisms of work hardening, dynamic recovery and recrystallization and may increase (as with Al-Fe) or remain

constant (as with Al). The cell size increase in alloys during the DLTR region may be rationalized by considering the factors which can enhance the cell or subgrain boundary migration. It is speculated that stress induced boundary migration is a good possibility which can also explain the delay for the appearance of the DLTR region to a higher wire drawing strain in Al-0.6Fe alloy due to the pinning effect of the boundaries by the precipitates. There is a general trend toward cleaner "cells" with sharper boundaries as the average size increases both with strain and as a function of alloying. Aluminum had least fraction of sharp high angle boundaries; sharpness and size increased in the order Al, EC-Al, Al-Mg, Al-Fe.

Dynamic recrystallization is a well documented phenomenon. It occurs during high temperature deformation [2] and has also been noted during high strains at low temperatures [9]. It is important to note the differences in structures produced by DLTR and static recrystallization. Static recrystallization progresses non-homogeneously. A partially recrystallized structure would contain a non-uniform distribution of sizes and misorientations. DLTR on the other hand proceeds uniformly with respect to size and misorientation.

The structures produced in this study should be compared with those in other deformation regimes and with other materials. High temperature deformation characteristically produces steady state microstructures at relatively low strains either through

dynamic recovery (high stacking fault energy) or dynamic recrystallization (low stacking fault energy) [2]. For dilute aluminum alloys the steady state is a relatively large subgrain structure produced by dynamic recovery and consisting entirely of low angle boundaries. This work shows that at room temperature steady state is not achieved though recovery and dynamic recrystallization takes place with grain structures much finer ($< 1\mu$) than those produced by high temperature dynamic recrystallization. Even though softening may occur (Al-Fe) a true steady state is not achieved up to strains of 5. The occurrence of DLTR limits the finest cell size that can be obtained. In BCC Fe, continued cell refinement occurs to an $\varepsilon = 7$ [25].

Analytical correlation between microstructural changes during drawing and the accompanying tensile flow stress behavior requires recognition and separation of the various stages just discussed.

As mentioned earlier, stage I consists of dislocation multiplication, formation of tangles and eventual appearance of a distinct cellular structure. Even though no quantitative microstructural data was obtained on the dislocation density for this stage, it is well established that hardening can be described by [35],

$$\sigma_f = \sigma_o + \alpha G b (\rho)^{\frac{1}{2}} \tag{4}$$

where α = flow stress; G = shear modulus

α_o = frictional stress; b = Burgers Vector

α = geometric constant; ρ = dislocation density

Equation (4) describes the strengthening contribution from both statistical and geometrically necessary dislocations [35]. If a distinction is made between the two densities, ρ_G and ρ_s and if they are properly weighted by their volume fraction [34], a grain size dependence on flow stress is predicted (i.e., $d^{\frac{1}{2}}$ dependence, where d is the original grain size). (Thompson et al. [34] have clearly demonstrated that work hardening is little affected by grain size in aluminum.) Thus it is speculated that in stage I, equation (4) should describe predominantly the work hardening produced by the statistical dislocation density which eventually forms the cell structure leading into stage II.

The strengthening in stage II is dominated by a dislocation cell structure of low angle boundaries and decreasing cell size. These dislocations constitute a statistical population generated during drawing. Holt [33] has analyzed such populations and found that $(\rho_s)^{\frac{1}{2}}$ is proportional to the reciprocal of the slip length, i.e.,

$$(\rho_s)^{\frac{1}{2}} = \frac{K'}{\lambda_s} \tag{5}$$

combining with equation (4), it gives

$$\sigma = \sigma_o + \frac{K_1}{\lambda_s} \tag{6}$$

This equation now relates the tensile flow stress to slip length. Obviously λ_s is a function of tensile straint (ε) and the original cell size ($\bar{L}$) generated during drawing. Since no theoretical basis exists for the functional relationship between λ_s, ε and $\bar{L}$, the following form is assumed

$$\lambda_s = \frac{1}{A + B\ \varepsilon^n} + C \tag{7}$$

where A, B and C are constants dependent on $\bar{L}$ and n is independent of $\bar{L}$. Note that from equation (7)

$$\lambda_s \to C \text{ as } \varepsilon \to \infty$$

$$\lambda_s \to \frac{1}{A} + C \text{ as } \varepsilon \to o$$

The variation of λ_s with ε is shown graphically in Figure 29. To allow for a dependence on $\bar{L}$, the constants A, B and C are assumed to have the form

$$A = \frac{C_1}{\bar{L}}\ ,\ B = \frac{C_2}{\bar{L}} \text{ and } C = C_3\bar{L} \tag{8}$$

where C_1, C_2 and C_3 are now material constants which are fixed for the alloy and independent of ε and $\bar{L}$. Note that this form allows for the cell boundaries to be penetrated depending on the values of C_1 and C_3. Substituting (8) in (7)

$$\lambda_s = \frac{1}{\frac{C_1}{\bar{L}} + \frac{C_2}{\bar{L}} \varepsilon^n} + C_3 \bar{L} \tag{9}$$

then at any strain ε

$$\lambda_s = K_2 \bar{L} \tag{10}$$

where

$$K_2 = \frac{1 + C_1 C_3 + C_2 C_3 \varepsilon^n}{C_1 + C_2 \varepsilon^n} \tag{11}$$

combining (10) and (6)

$$\sigma = \sigma_o + K_3 \bar{L}^{-1} \tag{12}$$

where

$$K_3 = \frac{(C_1 + C_2 \varepsilon^n) K_1}{1 + C_1 C_3 + C_2 C_3 \varepsilon^n} \tag{13}$$

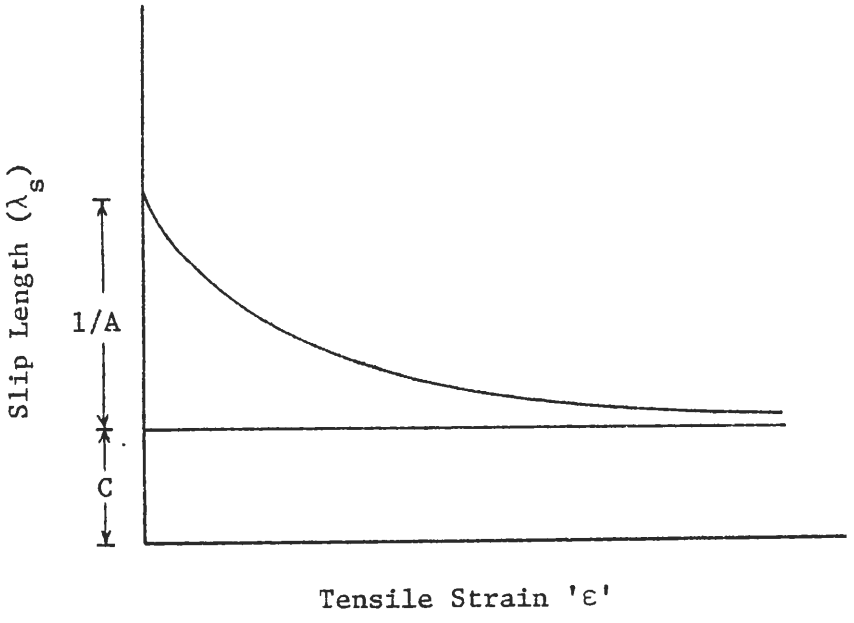

Figure 29. Schematic Variation of Slip Length, λ_s with Strain, ε

The equation (12) is a modified Hall-Petch relation. Similar equations have been derived by several authors in a variety of ways. The specific approach used here will allow a correlation between the modified Hall-Petch equation and the Hollomon equation as will be shown later.

It will be recalled that the low angle boundary substructures of stage II occur between strains of 0.5 to 1.5 in pure aluminum, 0.3 to 1.5 in Al-0.2Mg alloy, 0.3 to 2.6 in Al-0.6Fe alloy and 0.5 to 2.6 in EC aluminum. The corresponding 0.2% flow stress and cell size for these respective strains were fit to the modified Hall-Petch equation (12) and are shown in Figure 30. The high angle structures of the DLTR region (stage III) are not included in this plot. There are some important observations that can be made from Figure 30: (i) Between the cell sizes of 1.0 and 0.45μ a least square fit to equation (12) can be made for all the alloys. This gives K_3 = 4.30 KSI-μ and σ_o = 7.63 KSI. (ii) A break in the curve occurs at $\bar{L}$ = 0.45μ corresponding to a wire drawing strain of 1.47 for EC and Al-0.6Fe alloys. (iii) Date from statically annealed EC Al obtained from an earlier study [29] fits the extending portion of the curve beyond the break, i.e., low angle "cell" structures produced by cold drawing beyond $\varepsilon > 1.47$ (but less than that required to product DLTR) produce a similar strengthening effect to that of statically annealed "subgrains."

The break in the σ vs. "cell" size curve is important because it signifies a transition from a pure dislocation cell structure to

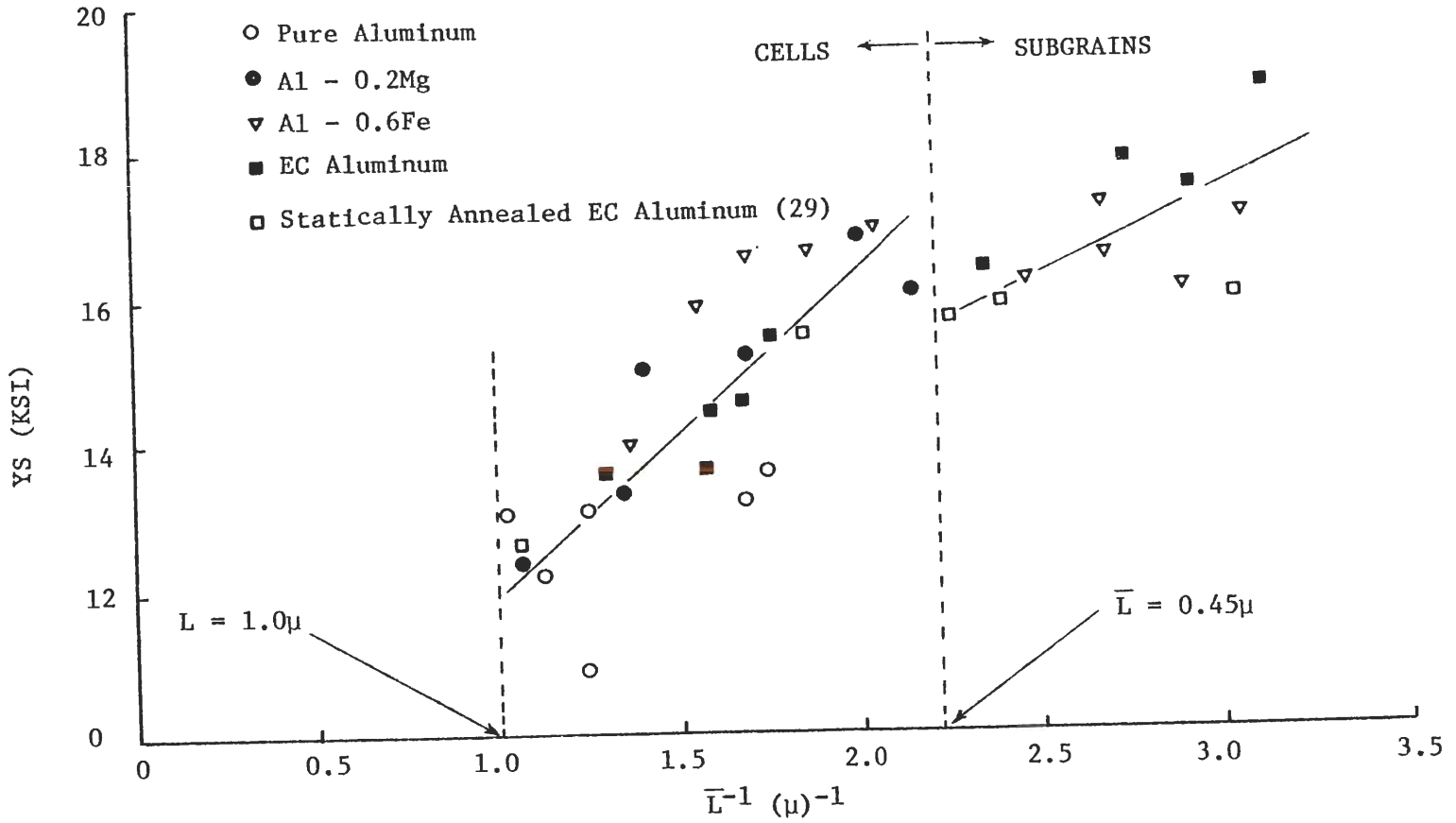

Figure 30. Modified Hall-Petch Plot for Pure Aluminum, Al-0.2Mg, Al-0.6Fe and an EC Aluminum. The Figure Includes the Data for Low Angle Cell Boundaries Only

a recovered subgrain structure. Such a transition would be expected on route to dynamic low temperature recrystallization (DLTR). The fact that the transition does not appear as dramatically with Al and Al-Mg as it does with EC and Al-Fe is not readily explanable in terms of dilute alloying effects on low temperature dynamic recovery; however, it should not be surprising that small variations in alloying will either extend or suppress the subgrain region. In previous work on conductor grade aluminum alloys [12] a single $(\bar{L})^{-1}$ line was fit to structures produced by combinations of cold drawing and static annealing. A break such as that shown in Figure 30 was not noted in that study since the conditions were neither as carefully controlled nor as explicit.

Much has been written about the proper value of the exponent in equation (12) with various authors using values ranging from -1 to $-\frac{1}{2}$. Figure 31 is included to show that a linear plot of σ vs. $(\bar{L})^{-\frac{1}{2}}$ can be obtained with the same data. The exact value of the exponent is not as important as the break in the σ vs. $\bar{L}$ relation. Rack and Cohen have noted a similar transition in heavily drawn iron as the recovery temperature is increased [24].

The greater strengthening effectiveness of cells over subgrains in the size range $\bar{L} < 0.4\mu$ has also been noted by Young and Sherby [4] and is summarized in the diagram reproduced in Figure 32. This behavior may be rationalized in a qualitative way by accepting the subgrain region as a stage of recovery in which the various constants of equation (8) takes on different values. This is equivalent to

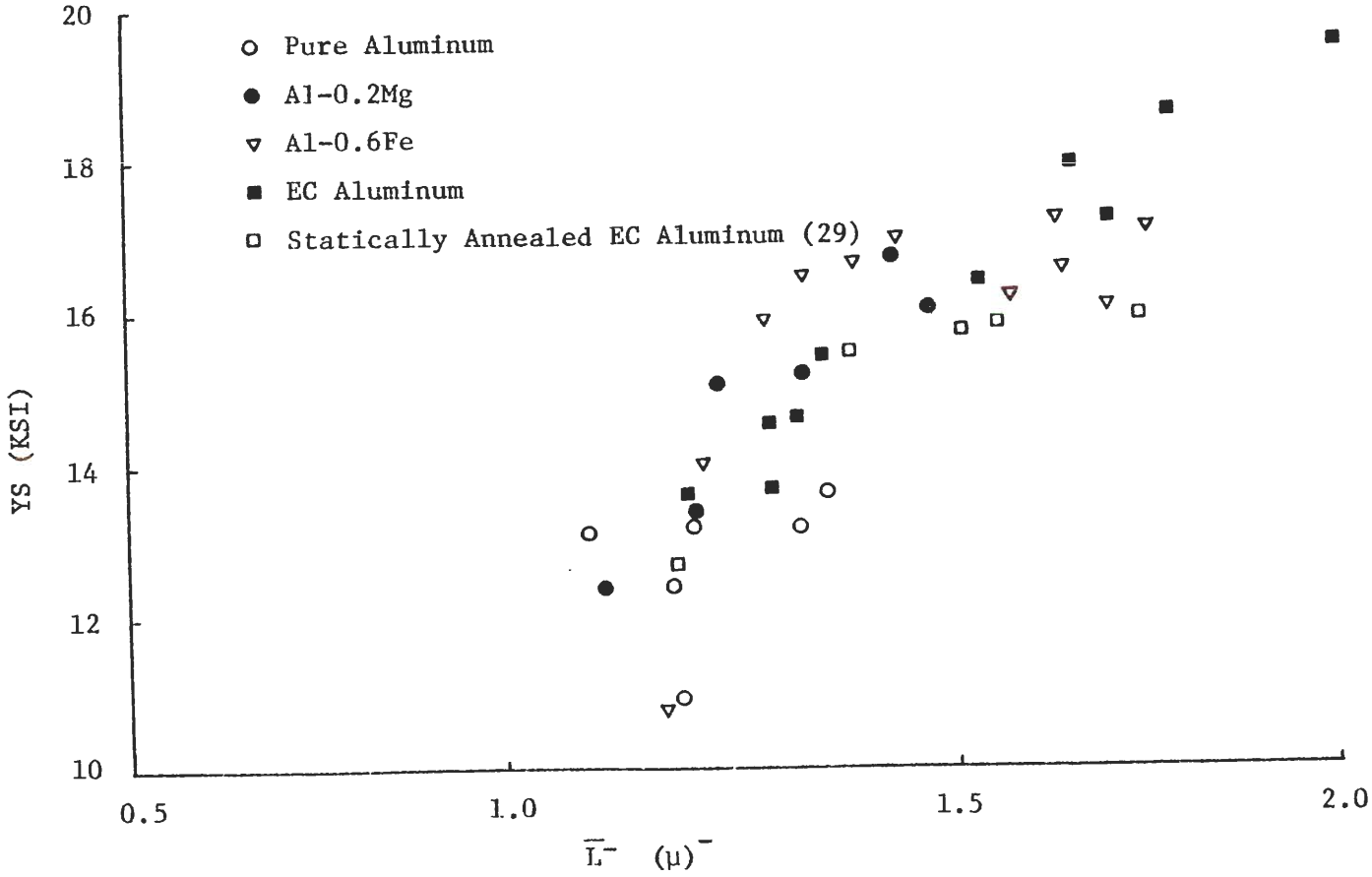

Figure 31. Hall-Petch Plot for Pure Aluminum, Al-0.2Mg, Al-0.6Fe and an EC Aluminum. The Figure Includes the Data for Low Angle Cell Boundaries Only

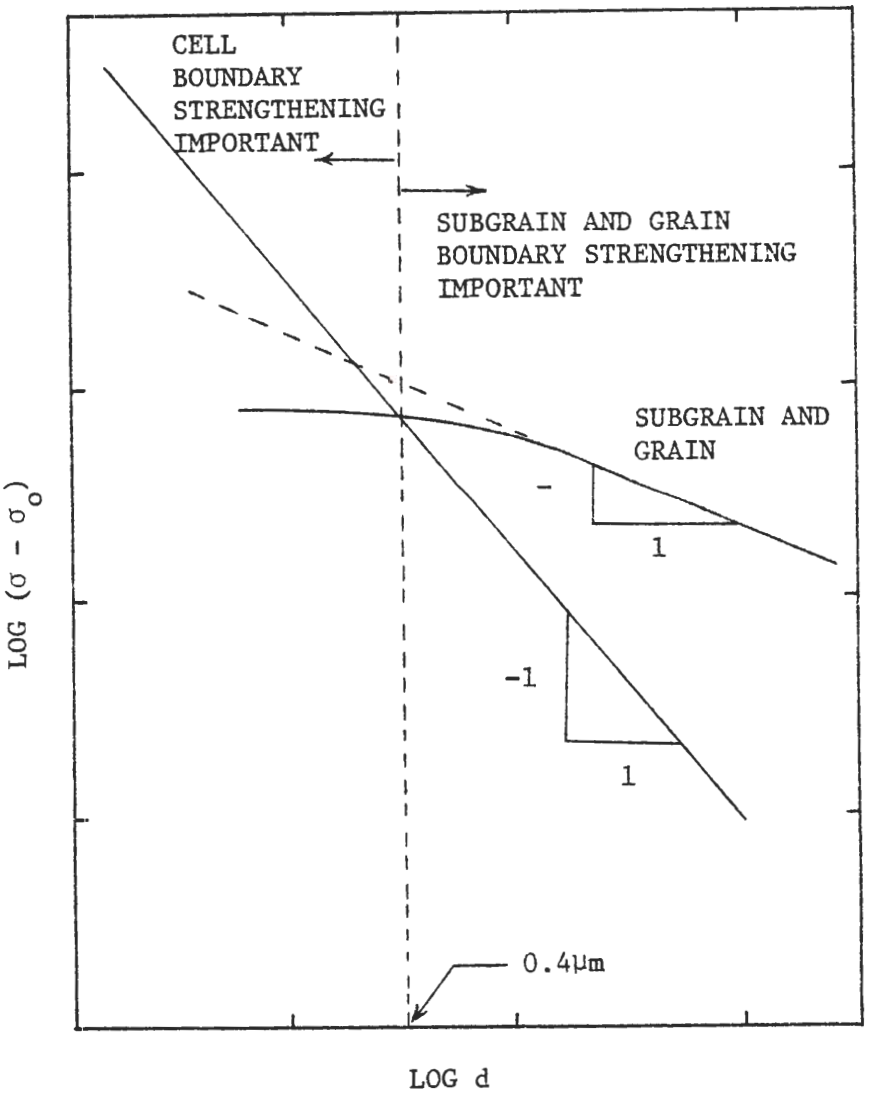

Figure 32. Schematic Representation of Strengthening Due to Grains and Cells. From Young and Sherby [4]

saying that the slip length in tension begins to depend in a different way on the "cell" size produced in wire drawing. In particular the boundaries become more penetrable as the redundant dislocations "clean up" in the subgrain region. Figure 30 also suggests that there is a limit to the strengthening attainable by cell size refinement as predicted by Thompson [7], without changing its boundary character. It is substantiated by the fact that, during the deformation, as the rate of dynamic recovery increases the redundant dislocations are reduced which results in the formation of subgrains. These subgrains are relatively recovered substructure having sharper boundaries compared to cells whose boundaries consist of tangled dislocations. The subgrain structure is less effective due to the presence of larger source lengths in its boundaries [32] as indicated by a lower slope for $\overline{L} < 0.45\mu$ in Figure 30.

The analysis applied to this point assumes a statistical dislocation density produced by wire drawing. It indicates that minor alloying may affect the relationship between cell boundary spacing and strain but a single functional relationship exists between σ and $\overline{L}$ in the range of 1 to 0.45μ. Beyond that point the boundaries take on a subgrain character and are less effective in strengthening due to changes in source lengths in the boundaries [6]. At still higher drawing strains dynamic low temperature recrystallization (DLTR) begins and the structure enters stage III.

The relationship between microstructure and flow stress in stage III cannot be easily treated analytically. A major difficulty

is the fact that the structure consists of a mixture of three types of boundaries: newly formed dislocation cell boundaries; recovered subgrain boundaries, and recrystallized high angle grain boundaries. The balance between work hardening, dynamic recovery and DLT recrystallization determines the distribution of boundary character, misorientation and size. Either the flow stress or the average "cell" size in this region may increase, remain constant or decrease and the two do not bear a simple relationship to one another (e.g., in Al-Mg, σ and $\bar{L}$ increase together and in Al-Fe σ decreases while $\bar{L}$ increases). A proper analysis would require detailed cell mapping similar to that done by Langford and Cohen [15].

A summary of the relationship between flow stress and average "cell" size for the different alloys of this study are shown in Figure 33. The various microstructural stages--cells, subgrains, and DLT recrystallization are indicated on the plots. The subgrain region is compressed in Al and Al-Mg but very distinct in Al-Fe and EC-Al. In all these alloys either the structure or the flow stress continues to change up to strains of 5. Additional data obtained on Al and Al-Fe to strains of 7 indicated that work hardening or softening was approaching saturation as shown in Figure 34. Achievement of a true steady state microstructure at this point is a possibility although detailed structural analysis beyond $\varepsilon = 5$ was not carried out.

The preceding analysis relates the flow-stress (0.2%) to a structural parameter ($\bar{L}$) at a fixed wire drawing strain. An

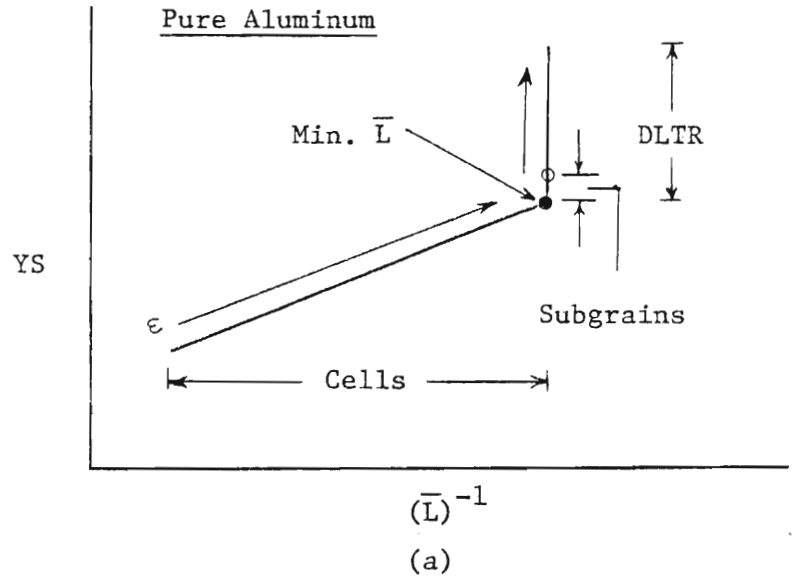

Figure 33. Schematic Modified Hall-Petch Plot for (a) Pure Aluminum, (b) Al-0.2Mg, (c) Al-0.6Fe and (d) EC Aluminum

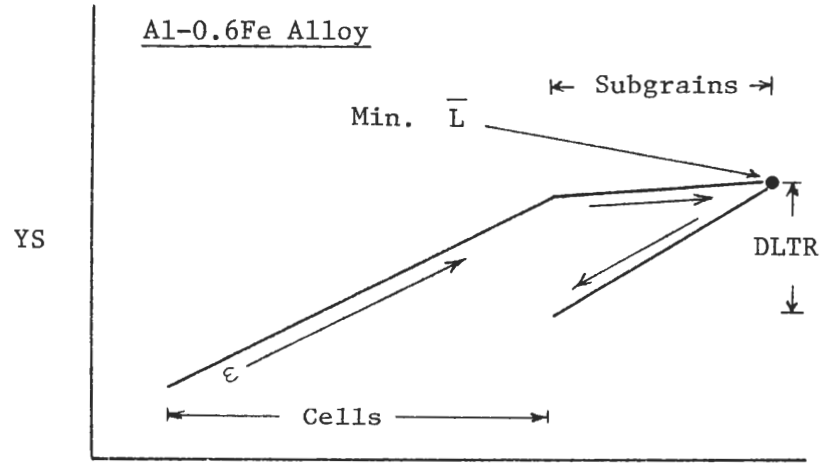
Al-0.6Fe Alloy
← Subgrains →
Min. $\bar{L}$
YS
DLTR
ε
Cells
$(\bar{L})^{-1}$

(c)

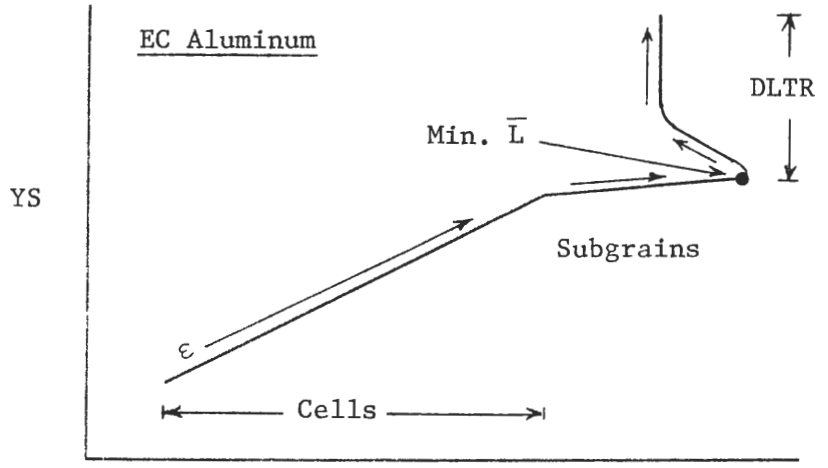
EC Aluminum
DLTR
Min. $\bar{L}$
YS
Subgrains
ε
Cells
$(\bar{L})^{-1}$

(d)

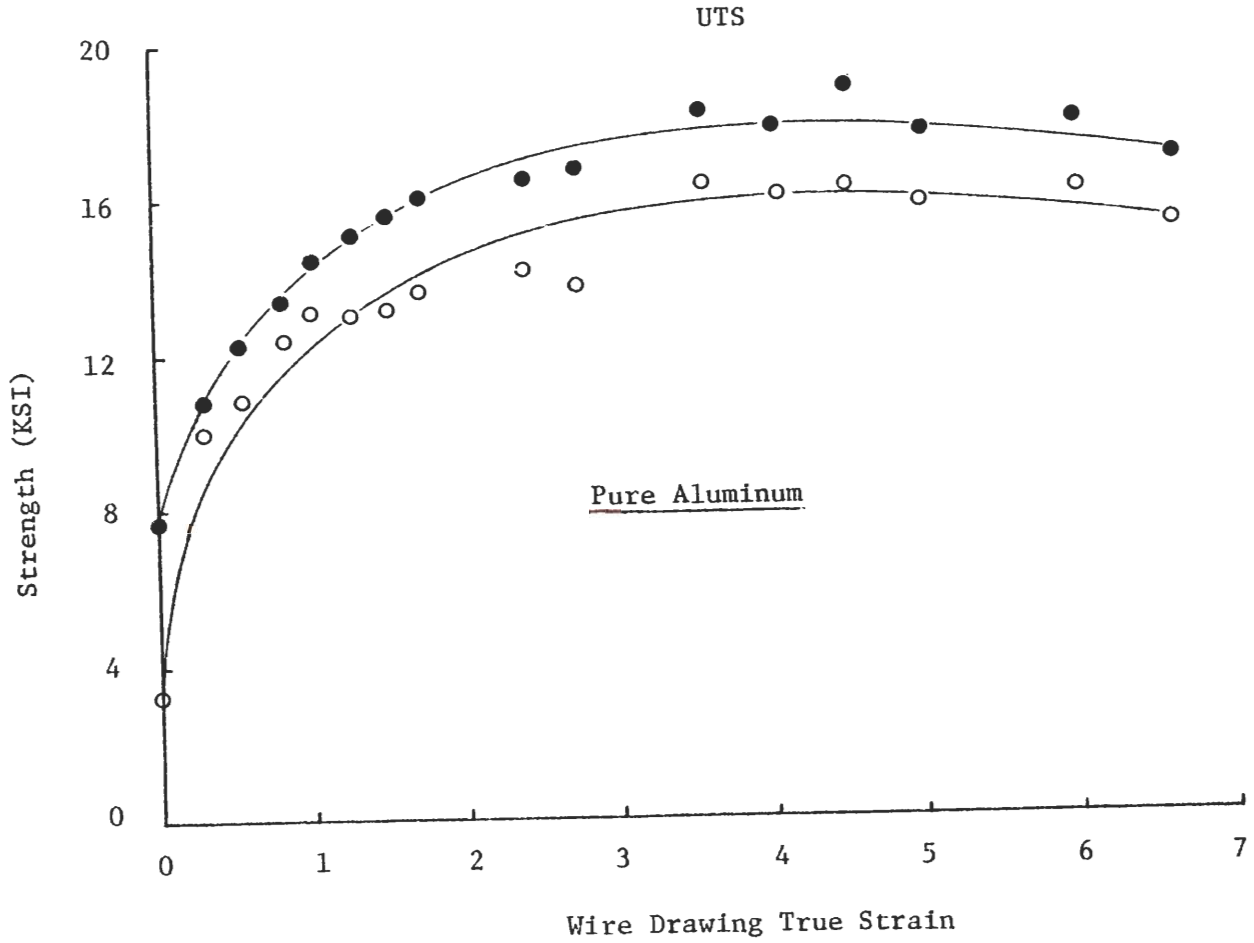

Figure 34. (a) Strain Hardening Envelop of Cold Drawn Pure Aluminum Up to a True Wire Drawing Strain of 7

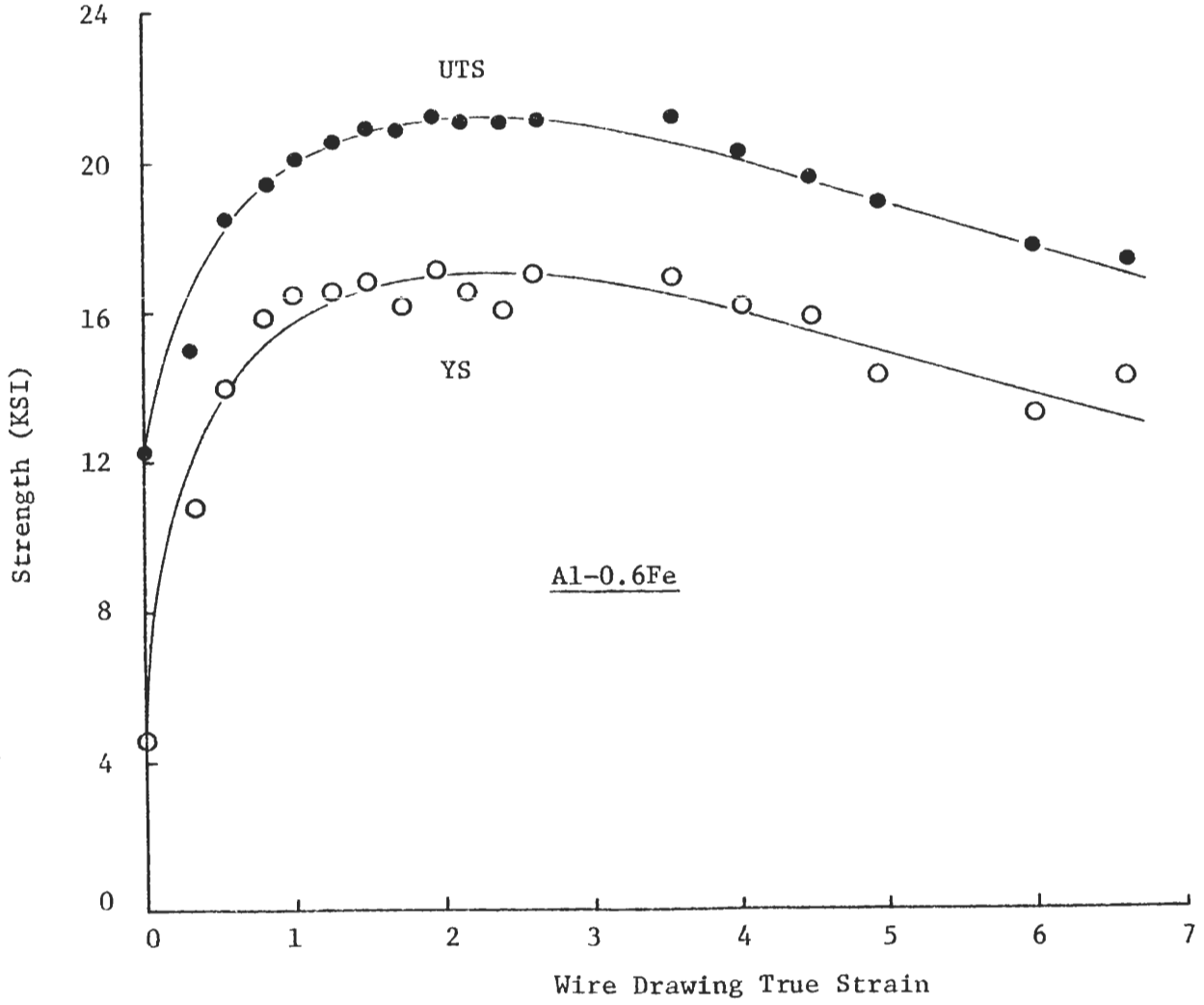

Figure 34. (b) Strain Hardening Envelop of Cold Drawn Al-0.6Fe Alloy Up to a True Wire Drawing Strain of 7.

alternative approach is to examine the form of the tensile σ vs. ε curve at a fixed microstructure. Consider first stage II, combining equations (12) and (13) which gives

$$\sigma = \sigma_o + \frac{K_1 C_1}{\bar{L}(1 + C_1 C_3 + C_2 C_3 \varepsilon^n)} + \frac{K_2 C_2 \varepsilon^n}{\bar{L}(1 + C_1 C_3 + C_2 C_3 \varepsilon^n)} \quad (14)$$

Since C_3 is the ratio of the final cell size (as tensile $\varepsilon \to \infty$) to the initial cell size (produced by wire drawing-characteristic of the tensile sample of $\varepsilon = o$) it can be considered as very small and the cell size produced by tensile strain could in principle be very low if DLTR did not intercede and the term $C_2 C_3 \varepsilon^n$ can be dropped out. This gives

$$\sigma = \sigma_o + \frac{K_1 C_1}{\bar{L}(1 + C_1 C_3)} + \frac{K_1 C_2}{\bar{L}(1 + C_1 C_3)} \varepsilon^n \quad (15)$$

The first term is the lattice friction stress and is independent of strain and structural parameters. The second term depends on cell size but not on ε while the third term depends on both. It should be noted that equation (15) is a generalized form of Ludwik equation [65, 68], but has been derived for the case of subgrain structures here. If it is assumed that the first and second terms are small in comparison to the third term, a simplest form that can be derived is the following equation, i.e.,

$$\sigma = K_4 \varepsilon^n \quad (16)$$

where

$$K_4 = \frac{K_1 C_2}{\bar{L} (1 + C_1 C_3)} \tag{17}$$

This approach of fitting the $\sigma = K\varepsilon^n$ curve to equation (16) has been taken by Cains et al. [9] to relate the variations of K_4 and n to microstructural changes in heavily rolled Cu. Equation (16) is an approximation since the neglected terms of equation (15) are sizable and structure dependent. Nonetheless it predicts that a fit of the various tensile stress-strain curves to the Hollomon equation should give K_4 values which vary inversely with $\bar{L}$. The variation of K with $\bar{L}$ has been discussed individually for the different alloys in previous sections. In general K and $\bar{L}$ do vary inversely in stage II as predicted, while n remained structurally insensitive. The variation of K with ε and $\bar{L}$ is reproduced by Al-0.6Fe alloy in Figure 35 with various microstructural regions designated. The inverse relation between K and $\bar{L}$ in cell refinement region is understandable from the proceding derivation. But the derivation also suggests that the transition from "cells" to "subgrain" should be indicated by a break in the curve for K vs. $\bar{L}^{-1}$ (since the constants C_1 and C_3 change with the character of the cell boundary). Thus it appears that K is not structurally sensitive enough to show a big effect of the break in the transition from "cells" to "subgrains." The variation of K with $\bar{L}$ in DLTR region therefore does not lend itself to an easy analysis.

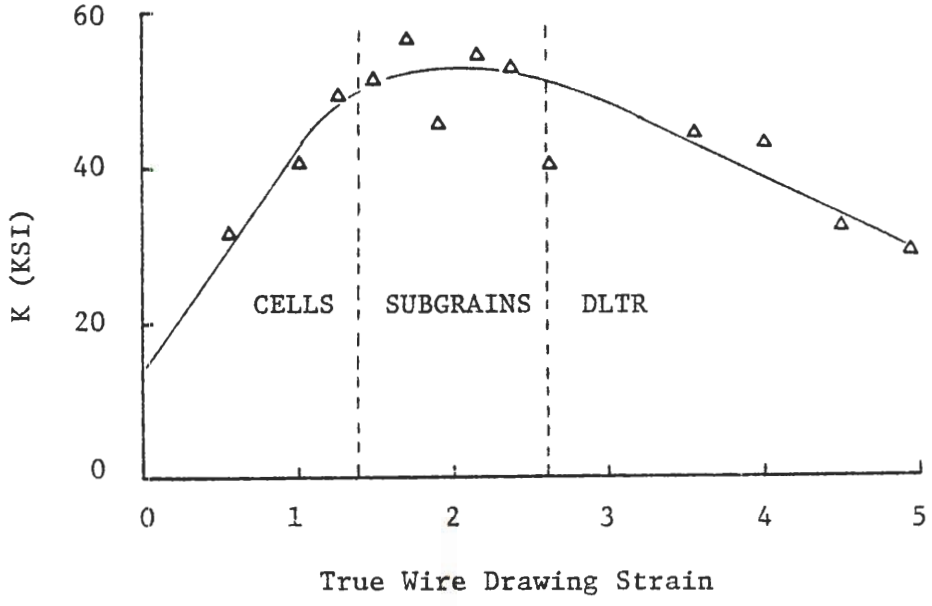

(a)

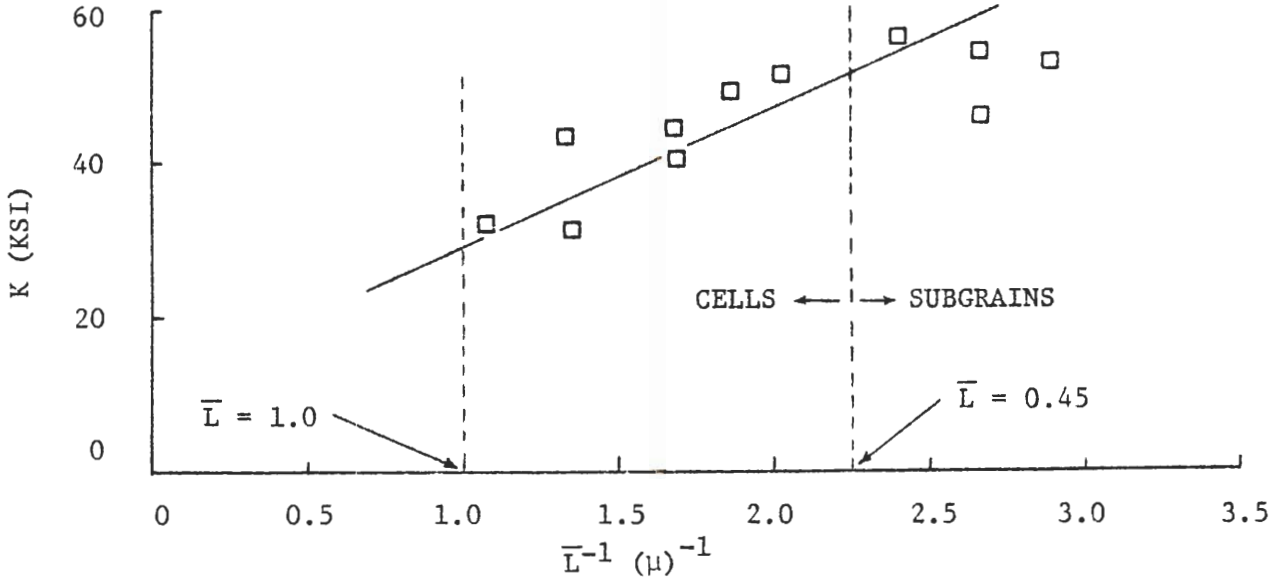

(b)

Figure 35. Variation of K with (a) True Wire Drawing Strain and (b) the Inverse of the Cell Size. The Figure Shows the Various Microstructural Regions

CHAPTER V

CONCLUSIONS

Dilute conductor grade aluminum alloys show the following strength and microstructural characteristics during wire drawing at room temperature:

1. Changes in either strength levels or microstructures continue to take place to strains as high as $\varepsilon = 5$ without the achievement of a dynamic steady state. Rapid hardening occurs up to $\varepsilon = 0.5$ followed by a decreasing hardening rate and either linear hardening or eventual work softening. Pure aluminum, Al-0.2Mg alloy and EC aluminum harden linearly with modulii of 1.0, 2.28 and 2.16 KSI respectively. In Al-0.6Fe work softening occurs between $2.3 < \varepsilon < 4.95$. There are indications of a steady state flow stress approaching at approximately $\varepsilon \geq 7$ in pure aluminum and Al-0.6Fe alloy.

2. Microstructural changes occur in the following sequence with increasing strain: dislocation multiplication → cell size refinement → subgrain formation → dynamic low temperature recrystallization (DLTR). Cell or subgrain structures are characterized by low angle boundaries (<10°) while DLTR structures are characterized by high angle boundaries. The cell and subgrain structures are differentiated by the character of their boundaries (source lengths being longer in subgrain). This behavior differs

from that at high temperatures when a steady state low angle subgrain structure occurs at moderate strains and dynamic recrystallization is not observed. The DLTR structure differs from that produced by static recrystallization in that it is much finer (grain sizes less than 0.5μ) and evolves more uniformly without distinct nucleii. A simple <111> texture develops and sharpens to the highest measured strains in all the alloys studied.

3. Small amounts of Mg and Fe promote the onset of cell formation. The subgrains region is quite small in pure aluminum and Al-0.2Mg alloy but is extended and made more distinct by the presence of Fe. Cells occur in the size range of 1 to 0.45 and subgrains from 0.45 to 0.25 .

4. Two distinct modified Hall-Petch relations are required for the cell and subgrain structures. In each region the flow stress and average cell size may be related by

$$\sigma = \sigma_o + k\ (\bar{L})^{-m}$$

where m = 1 or ½. Value of k is much smaller for the subgrains indicating that they are less effective as strengthening barriers. In the cell structure region all four materials can be fit to a common $(\bar{L})^{-1}$ plot indicating that small additions of soluble an insoluble additions to aluminum may affect the rate of cell formation and refinement, but not the relationship between

substructure and strength. Knowledge of the statistical misorientation of the subgrains is necessary to evaluate the strengthening in DLTR region.

5. When the complete tensile stress-strain curves at various wire drawing intervals are fit to the Hollomon equation, $\sigma = \varepsilon^n$, K is found to vary inversly with the average effective "cell" size even in the DLTR region. No distinct breaks are seen in the variation of $\bar{L}$ with K. Values of n vary between 0.05 to 0.20 and does not vary systematically with structure.

BIBLIOGRAPHY

1. R. J. McElroy and Z. C. Szkopiak, Int. Met. Rev., 17, 167 (1972), 175.

2. H. J. McQueen and J. J. Jonas, "Recovery and Recrystallization During High Temperature Deformation," in Treatise on Mat. Sci. and Tech., 6, Academic Press, San Francisco. (1975)

3. C. M. Sellars and W. J. McG. Tegart, Int. Met. Rev., 17, 158 (1972).

4. C. M. Young and O. D. Sherby, J. Iron and Stell Inst., (1973) 630.

5. "Mechanical-Thermal Processing and Dislocation Substructure Strengthening," IMD/TMS-AIME Symposium, Las Vegas (1975).

6. A. W. Thompson, Acta Met., 23, (1975) 1337.

7. A. W. Thompson, Met. Trans., 8A, (1977) 833.

8. O. D. Sherby, R. H. Klundt and A. K. MIller, Met. Trans., 8A, (1977) 843.

9. J. H. Cairns, J. Clough, M. A. P. Dewey and J. Nutring, J. Inst. Met., 99, (1971) 93.

10. B. A. Wilcox and A. H. Clauer, Acta Met., 20, (1972) 743.

11. D. J. Abson and J. J. Jonas, Met. Sci. J., 4,(1970) 24.

12. D. Kalish and B. G. LeFevre, Met. Trans., 6A, (1975) 1139.

13. M. R. Staker and D. L. Holt, Acta Met., 20, (1972) 569.

14. H. J. Rack and M. Cohen, Frontiers in Mat. Sci. Marcel Dekkar, N. Y., (1974).

15. G. Langford and M. Cohen, Met. Trans., 6A, (1975) 901.

16. D. J. Michel, J. Mateff and A. J. Lovell, Acta Met., 21, (1973) 1269.

17. H. J. McQueen, Met. Trans., 8A, (1977) 807.

18. C. M. Young, S. L. Robinson and O. D. Sherby, Acta Met., 23, (1973) 633.

19. V. V. Levitin and L. K. Orzkitskaya, Fiz. Metal Metalloved, 4, (1973) 149.

20. J. Weertman, Trans. ASM, 61, (1968) 681.

21. L. J. Cuddy, Met. Trans., 1, (1970) 395.

22. G. Laird, "Substructure Sensitivity of Fatigue" in References.

23. C. M. Young, C. J. Anderson and O. D. Sherby, Met. Trans., 5, (1974) 519.

24. H. J. Rack and M. Cohen, Mat. Sci. & Eng., 6, (1970) 320.

25. G. Langford and M. Cohen, Trans. ASM, 62, (1969) 623.

26. J. D. Embury, A. S. Keh and R. M. Fisher, Trans. Met. Soc. AIME, 236, (1966) 1252.

27. J. Nutting, Eight Int. Cong. on Elec. Mic., Conberra, 1, (1974) 581.

28. A. S. Malin and M. Hatherly, Eight Int. Cong. on Elec. Mic., CAnberra, 1, (1974) 582.

29. D. Kalish, B. G. LeFevre and S. K. Varma, Met. Trans., 8A, (1977) 204.

30. S. F. Exell and D. H. Warrington, Phil. Mag., (1972) 1121.

31. J. E. Bird, A. K. Muklerjee and D. E. Dorn, "Quant. Relation Between Properties and Microsturcture," Bradon and Rasen, eds., (1969) 255.

32. D. Kuhlman-Wilsdorf, Met. Trans., 1, (1970) 3173.

33. D. L. Holt, J. Appl. Phys., 4., (1970) 3197.

34. A. W. Thompson, M. I. Baskes and W. F. Flanagan, Acta Met., 21, (1973) 1017.

35. M. F. Ashby, Phil. Mag., 21, (1970) 399.

36. J. S. H. Lake and G. B. Craig, Trans. ASM, 61, (1968) 829.

37. D. Kuhlman-Wilsdorf, Trans. Met. Soc. AIME, 224, (1962) 1047.

38. A. S. Keh and S. Weissman, "Elec. Mic. and Strength of Crystals," R. R. Swann, ed., Interscience Publ., N. Y. (1963) 231.

39. H. Fujita and T. Tabata, Acta Met., 21, (1973) 355.

40. A. W. Thompson and H. J. Saxon, Met. Trans., 4, (1973) 1599.

41. G. Langford, P. K. Nagata, R. J. Sober and W. C. Leslie, Met. Trans., 3, (1972) 1843.

42. O. D. Sherby and C. M. Young, "Rate Processes in Plastic Flow," Li and Mukherjee, ed., Am. Soc. of Met. (1975).

43. J. E. Hockett and O. D. Sherby, J. Mech. Phys. Sol., 23, (1975) 87.

44. G. I. Taylor and H. Quinney, Proc. Roy. Soc., A143, (1933) 30.

45. S. J. Thompson and P. Flewitt, J. Less Comm. Met., 40, (1975) 269.

46. R. R. Westerlund and N. T. Bond, Wire Journal, Oct. 1973, 91.

47. J. Gil-Sevillano and E. Aernoudt, Met. Trans., 6A, (1975) 2163.

48. C. M. Young, L. J. Anderson and O. D. Sherby, Met. Trans., 6A, (1975) 2163.

49. H. G. Grewe and E. Kapler, Phy. Stat. Sol., 6, (1964) 669.

50. F. E. Feltner and C. Laird, Acta Met., 15, (1967) 1633.

51 J. J. Jonas, C. M. Sellars and W. J. McG. Tegart, Met. Rev., 130, (1969) 1.

52. J. J. Jonas, H. J. McQueen and W. A. Wong, ISI Publication, 108, (1968) 49.

53. H. J. McQueen, J. of Metals, Apr. (1963), 31.

54. C. Biswas, M. Cohen and J. F. Breedis, "Microstructures and Design of Alloys, 1, (1973) 16.

55. W. G. Truckner and D. E. Mikkola, Met. Trans., 8A, (1977) 45.

56. Jean Howard, Scripta Met., 10, (1976) 441.

57. E. H. Chia, Ph. D. Dissertation, Georgia Institute of Technology, (1975).

58. E. H. Chia and E. A. Starke, Jr., Met Trans., 8A, (1977) 825.

59. W. A. Backofen, "Deformation Processing," Addison Wesley, Reading, Mass., (1972).

60. U. F. Kocks, Met. Trans., 1, (1970) 1121.

61. E. P. Abrahamson, "Influence of Grain Refinement on Some Mechanical Properties," in Surf. & Interf. II, Syracuse University Press, (1968) 262.

62. W. B. Morrison, Trans. ASM, 59, (1966) 824.

63. D. C. Ludwigson, Met. Trans., 2, (1971) 2825.

64. Kanji Ono, Met. Trans., 3, (1972) 749.

65. A. W. Bowen and P. G. Partridge, J. Phys. D:Appl. Phys., 7, (1974) 969.

66. H. J. Kleemola and M. A. Nielineu, Met. Trans., 5, (1974) 1963.

67. J. R. C. Guimaraes, Scripta Met., 8, (1974) 912.

68. D. V. Wilson, J. Phys. D:Appl. Phys., 7, (1974) 954.

69. J. R. Cotner and W. J. McG. Tegart, J. Inst. Metals, 97, (1969).

70. M. J. Lutron and C. M. Sellars, Acta Met., 17, (1969) 1033.

71. S. Fulop and H. J. McQueen, Super Alloys: Processing, Metals-Ceramics Information Center, Columbus, (1972) H1.

72. J. P. A. Immarigeon and J. J. Jonas, Acta Met., 19, (1971) 1053.

73. R. W. Westerlund, Met. Trans., 5A, (1974) 667.

74. S. C. Dexter and I. G. Greenfield, Met. Trans., 2, (1971) 181.

VITA

Shailendra K. Varma was born in Lucknow, India on July 18, 1945. He graduated from D. A. V. Higher Secondary School, New Delhi, India in 1962. He received his B. E. degree in Metallurgical Engineering from University of Roorkee in 1967. He worked in Solid State Physics Laboratory, Delhi for nearly 2 years. He was involved in the research of Solid State Physics Laboratory in the field of growth of silicon single crystals by Czochralski and Float Zone methods, production of dislocation free single crystals of silicon and doping of silicon crystals with P, Sb and B. As a result of his work, he co-authored in three publications:

(i) "On Silicon Single Crystal Growth by Czochralski Method," Journal of Institution of Telecommunication Engineers, vol. 16, no. 9, 696-701, 1970.

(ii) "Silicon Single Crystals Almost Free of Dislocations," Journal of Crystal Growth, vol. 8, 223-225, 1971.

(iii) "On Doping of Silicon Crystals," Journal of Pure and Applied Physics, vol. 19, no. 2, 135-136, 1971.

He came to the U. S. A. in 1971 to join the University of Denver, Denver, Colorado, where he received his M. S. degree in Metallurgy and Materials Science in 1974. His M. S. thesis involved a study of the Lithium-Iridium-Hydrogen system. He enrolled in the Graduate Division of the Georgia Institute of Technology to pursue his Ph. D. degree in Metallurgy during 1974. As a graduate

student in the Metallurgy Program, School of Chemical Engineering he co-authored in the publication: "Effect of Alloying and Processing on Subgrain-Strength Relationship in Aluminum Conductor Grade Alloys," Metallurgical Transactions, vol. 8A, 204-206, 1977.

He is married to the former Ranjana Srivastava.